DOI: 10.26599/FSHW.2026.9251350

Contents lists available at SciOpen

Food Science and Human Wellness

journal homepage: https://www.sciopen.com/journal/2097-0765

China Food Publishing Co.

Atractylodes macrocephala Koidz. Polysaccharide Ameliorates Colitis via Microbiota-Independent Activation of Autophagy and Induction of Mucin 2 Secretion

Yimu Ma[1, †], Zhihua Wang [1, †], Yaqi Tong [1], Yonghong Chen[1], Yubo Xu [1], Mengji Liu [2], Qian Qu [1], Jianni Huang[3, *], Weijie Lv[1, *], Shining Guo[1, *]

[1] *College of Veterinary Medicine, South China Agricultural University, Guangzhou, China*

[2] *School of Animal Science and Technology, Foshan University, Foshan, China*

[3] *College of Animal Science and Technology, Guangxi University, Nanning, China*

ABSTRACT: Ulcerative colitis (UC) is a chronic inflammatory bowel disease featured by impaired colonic mucus barrier dominated by MUC2. Dietary polysaccharides alleviate UC mainly via gut microbiota fermentation, but their direct effects on goblet cells remain unclear. Here, we identified a low-molecular-weight (2.68 kDa) inulin-type fructan from *Atractylodes macrocephala Koidz*. (AMKP). In DSS-induced colitis model, AMKP administration significantly ameliorated clinical symptoms while robustly upregulating MUC2 expression. Crucially, the therapeutic benefits of AMKP and its promotion of MUC2 secretion persisted even after exhaustive microbiota depletion via antibiotic (ABX) treatment, suggesting a microbiota-independent mechanism. *In vitro* mechanistic assays using LS174T goblet cells revealed that AMKP directly stimulates MUC2 synthesis and secretion. Further investigation demonstrated that AMKP-mediated mucosal restoration is driven by the activation of autophagy and the subsequent alleviation of endoplasmic reticulum (ER) stress. Notably, through the use of the autophagy inhibitor 3-MA and the ER stress inducer TUN, we confirmed that AMKP's protective effect is strictly dependent on the autophagy-MUC2 axis. Our findings shift the paradigm of polysaccharide action from "microbial fermentation" to "direct host cell modulation". By identifying AMKP as a direct secretagogue for goblet cells, this study provides a novel, microbiota-independent therapeutic strategy for restoring intestinal homeostasis in UC.

Keywords: Inulin-Type Fructan; *Atractylodes macrocephala Koidz.;* Colitis; Autophagy; MUC2

1. Introduction

Ulcerative colitis (UC) is a chronic, relapsing inflammatory bowel disease characterized by diffuse colonic inflammation and a disrupted epithelial barrier [1]. Central to this barrier is the mucus layer, predominantly composed of the gel-forming mucin MUC2, which physically segregates the gut microbiota from the underlying epithelium [2]. In patients with UC, goblet cell dysfunction and MUC2 depletion led to bacterial translocation and sustained inflammation [3]. Consequently, restoring MUC2 production and mucus barrier integrity has emerged as a pivotal therapeutic goal.

† Yimu Ma and Zhihua Wang contributed equally.
***Corresponding author**
Shining Guo, shining@scau.edu.cn; Weijie Lv, lvwj@scau.edu.cn; and Jianni Huang, jiannihuang@gxu.edu.cn.

Received 24 April 2026
Received in revised from 12 June 2026
Accepted 31 July 2026

Dietary polysaccharides are widely recognized for their anti-inflammatory properties in UC, with the prevailing paradigm attributing their efficacy to gut microbiota-mediated fermentation and short-chain fatty acid production [4]. While several herbal polysaccharides upregulate colonic MUC2 expression, these effects are consistently reported to be microbiota-dependent [5-7]. However, this paradigm leaves a critical mechanistic gap: whether certain structurally unique polysaccharides can directly modulate goblet cell function independent of microbial biotransformation remains unknown.

Atractylodes macrocephala Koidz. is a classic 'medicinal and food homologous' herb used to fortify the spleen and gastrointestinal tract. Although its polysaccharides have been reported to alleviate colitis, the structural determinants and host-targeted mechanisms underlying their bioactivity are not fully elucidated [8, 9]. In particular, low-molecular-weight inulin-type fructans possess structural features that may confer resistance to upper gastrointestinal digestion, potentially enabling direct interaction with the intestinal epithelium.

Here, we hypothesized that a low-molecular-weight inulin-type fructan from *Atractylodes macrocephala Koidz.* (AMKP) can directly target intestinal goblet cells—independent of the gut microbiota—to promote MUC2 secretion through activation of autophagy and subsequent alleviation of endoplasmic reticulum (ER) stress, thereby ameliorating ulcerative colitis. To test this hypothesis, we integrated *in vivo* microbiota depletion models, *in vitro* simulated digestion, and pharmacological modulation of autophagy and ER stress in goblet cells. Our findings challenge the conventional "microbial fermentation" paradigm and establish AMKP as a direct goblet cell secretagogue, offering a novel microbiota-independent strategy for restoring intestinal homeostasis in UC.

2. Materials and methods

2.1 Materials

Atractylodes macrocephala Koidz. was purchased from Beijing Tongrentang Guangzhou Pharmaceutical Chain Co., Ltd (Guangzhou, China). DEAE Sepharose FF was purchased from Wuhan Huiyan Biotechnology Co., Ltd (Wuhan, China). The gel filtration medium Chromdex 75PG was purchased from Bestchrom Biotechnology Co., Ltd (Shanghai, China). The Dextran (molecular weight 1000–670000) series of analytical standards was purchased from Sigma-Aldrich (Germany). Monosaccharide standards, including fucose (Fuc), rhamnose (Rha), arabinose (Ara), galactose (Gal), glucose (Glc), xylose (Xyl), mannose (Man), fructose (Fru), ribose (Rib), galacturonic acid (Gal-UA), glucuronic acid (Glc-UA), mannuronic acid (Man-UA), and guluronic acid (Gul-UA), were purchased from Sigma-Aldrich (Germany). ABX (Vancomycin, Neomycin, Metronidazole, Ampicillin) were purchased from Shanghai Yuanye Bio-Technology Co., Ltd. (Shanghai, China). 3-Methyladenine (3-MA) and Tunicamycin (TUN) were purchased from MedChemExpress LLC (New Jersey, USA).

2.2 Extraction, isolation, and purification of polysaccharides

The polysaccharide extraction method was modified from the previously described procedure [10], as shown in Fig. 1A. Briefly, *Atractylodes macrocephala Koidz.* was crushed, defatted, and then subjected to

ultrasound-assisted water extraction. Ultrasound-assisted extraction was performed at a solid-to-liquid ratio of 1:10 (w/v) with a frequency of 59 kHz and a temperature of 50 °C for 20 min. This procedure was repeated twice, and the supernatants from both extractions were combined. The extract was concentrated, followed by alcohol precipitation. The precipitate was lyophilized, redissolved, and deproteinized. Subsequently, alcohol precipitation was performed again, and the final product was obtained by freeze-drying to yield the crude AMKP.

The crude AMKP was dissolved in distilled water and centrifuged (8000 × g, 10 min) to remove the precipitate. The supernatant was loaded onto an ion exchange chromatography column (DEAE Sepharose FF). After elution with different salt concentrations (dH_2O, 0.2M NaCl, 0.5M NaCl, 1.0M NaCl), the polysaccharide content in the eluates was detected by the anthrone-sulfuric acid method. The corresponding fractions were collected to obtain AMKP-E1. AMKP-E1 was dissolved in distilled water and loaded onto a gel filtration column (Chromdex 75PG), which was eluted with ultrapure water. The eluate was monitored online with a differential detector, and the elution peaks exhibiting higher intensity and better symmetry were collected. The eluate from the same peak region was pooled and lyophilized to yield AMKP.

2.3 Structural characterization of AMKP

2.3.1 Molecular weight analysis

Dextran standards with different molecular weights were used to prepare analytical standards, and a calibration curve was established using the HPGPC. The HPGPC analysis was performed using a tandem column system consisting of OHpak SB-803 HQ, OHpak SB-804 HQ, and OHpak SB-805 HQ (8 × 300 mm) with an aqueous polymer-based SEC (GFC) matrix. The mobile phase was 0.05 M NaCl solution at a flow rate of 0.65 mL/min, the column temperature was maintained at 40ºC, and the injection volume was 30 μL. The chromatogram of samples was obtained under these conditions. The molecular weight of the sample was calculated based on the calibration curve.

2.3.2 Monosaccharide composition analysis

Accurately weighed monosaccharide standards and polysaccharide samples were processed and dissolved in sterile water for chromatographic analysis. The analysis was performed using a Thermo ICS5000+ ion chromatography system (ICS5000+, Thermo Fisher Scientific, USA) equipped with a Dionex™ CarboPac™ PA20 (150 × 3.0 mm, 10 μm) liquid chromatography column. The injection volume was 5 μL. The mobile phases consisted of phase A (H_2O), phase B (0.1 M NaOH), and phase C (0.1 M NaOH, 0.2 M NaAc). The column temperature was maintained at 30°C, and the monosaccharide components were analyzed and detected using an electrochemical detector.

2.3.3 FT-IR analysis

AMKP and KBr powders were accurately weighed, thoroughly ground in a mortar, and pressed into a pellet. The sample was then scanned using a NICOLET iS50R Fourier Transform Infrared Spectrometer

(Thermo Scientific, USA) with a wavenumber range of 4000–400 cm^{-1}, and the infrared spectrum was recorded.

2.3.4 Methylation analysis

The derivatization procedure for the AMKP was consistent with that described in the report [11]. The processed sample was analyzed by gas chromatography-mass spectrometry (GC-MS). The chromatographic separation was performed using an Agilent gas chromatography system (Agilent 7890A; Agilent Technologies, USA) equipped with an HP-5MS capillary column (30 m × 0.25 mm × 0.25 μm, Agilent J&W Scientific, Folsom, CA, USA). High-purity helium (purity ≥ 99.999%) was used as the carrier gas at a constant flow rate of 1.0 mL/min. The injector temperature was set at 260°C. A 1 μL sample was injected in split mode with a split ratio of 10:1 and a solvent delay of 2.2 min. The temperature program was as follows: hold at 50°C for 1.0 min, increase to 130°C at a rate of 50°C/min, then increase to 230°C at 3°C/min, and finally hold at 230°C for 2 min. The mass spectrometric analysis was conducted using an Agilent quadrupole mass spectrometry system (Agilent 5977B; Agilent Technologies, USA) equipped with an electron impact ionization (EI) source and MassHunter workstation. The EI source conditions were as follows: ion source temperature 230°C, quadrupole temperature 150°C, and electron energy 70 eV. The analysis was performed in full scan (SCAN) mode with a mass scan range (m/z) of 30-600.

2.3.5 NMR analysis

AMKP was dissolved in 0.5 ml of D_2O. ^{1}H-NMR, ^{13}C-NMR, DEPT-135, and 2D NMR spectra (COSY, HSQC, HMBC, NOESY) were acquired using a 600 MHz Bruker NMR spectrometer (Bruker, Rheinstetten, Germany). Chemical shifts are reported in ppm and were referenced to the residual HDO signal (δ H = 4.70 ppm) for ^{1}H and to tetramethylsilane (TMS, δ C = 0.00 ppm) for ^{13}C.

2.4 Animal experiments

Male C57BL/6J mice aged 6-7 weeks were purchased from the Laboratory Animal Center of South China Agricultural University (Guangzhou, China). All experimental procedures in this study were approved by the Animal Ethics Committee of the South China Agricultural University (permit number: 2023b069, 2025b117, Guangzhou, China). All mice were raised under a 12 hours light/dark cycle at room temperature (23 ± 2°C) with access to food and water ad libitum. In the experiment, each mouse was considered an independent replicate. Mice were randomized to groups according to body weight so that the mean initial body weight was similar across groups. To meet statistical requirements, each group contained 6 mice. All experimental procedures were performed by trained personnel. Every effort was made to minimize animal suffering.

During the experiment, 3% DSS was administered ad libitum in drinking water, whereas ABX (Vancomycin, 100 mg/kg; Neomycin, 200 mg/kg; Metronidazole, 200 mg/kg; Ampicillin, 200 mg/kg) [12] and AMKP (100 mg/kg, 200 mg/kg, 400 mg/kg) [13] were given by oral gavage, and 10 mg/kg 3-MA [14] was

delivered via intraperitoneal injection to their respective treatment groups. Detailed animal procedures are as follows.

Exp. 1: Mice were divided into: (1) Con: sterile water (days 0–7) + saline (days 8–14); (2) DSS: 3% DSS (days 0–7) + saline (days 8–14); (3) DSS+PL: 3% DSS (days 0–7) + 100 mg/kg AMKP (days 8–14); (4) DSS+PM: 3% DSS (days 0–7) + 200 mg/kg AMKP (days 8–14); (5) DSS+PH: 3% DSS (days 0–7) + 400 mg/kg AMKP (days 8–14).

Exp. 2: Mice were divided into: (1) ABX+DSS: ABX (days -5–0) + 3% DSS (days 0–7) + saline (days 8–14); (2) ABX+DSS+AMKP: ABX (days -5–0) + 3% DSS (days 0–7) + 400 mg/kg AMKP (days 8–14).

Exp. 3: Mice were divided into: (1) DSS+AMKP: 3% DSS (days 0–7) + 400 mg/kg AMKP (days 8–14); (2) DSS+AMKP+3-MA: 3% DSS (days 0–7) + 400 mg/kg AMKP and 10 mg/kg 3-MA (days 8–14).

Body weight, stool consistency, and fecal occult blood were assessed daily. At the end of the study, mice were euthanized under anesthesia. Data points that deviated excessively from the group mean were excluded. Colon length and spleen weight were measured, and colon tissue along with fecal samples were collected for subsequent analysis.

2.5 In vitro digestion of polysaccharides

The in vitro digestion method followed previous reports [15]. Simulated gastric fluid and simulated intestinal fluid were prepared according to standard formulations. AMKP was subjected to digestion at 37°C with shaking at 120 rpm. Samples were collected after 0, 1, 2, and 4 h of gastric digestion, and after 0, 2, 4, and 6 h of sequential gastrointestinal digestion for reducing sugar assays. After 4 h of gastric digestion and 6 h of gastrointestinal digestion, samples were collected, lyophilized, and designated as G-AMKP and GI-AMKP, respectively, for HPGPC analysis. The reducing sugar content was determined using the DNS reagent method as previously described [16], and HPGPC analysis was performed as outlined in Section 2.3.1.

2.6 Cell culture and cell experiments procedures

LS174T cells were purchased from Procell Life Science & Technology Co., Ltd. (Wuhan, China). Cells were cultured in DMEM supplemented with 10% FBS and 1% penicillin−streptomycin. Cultures were incubated at 37 °C in a humidified atmosphere with 5% CO2. Cell viability of LS174T cells following 24 h of AMKP treatment was assessed using a CCK-8 assay. As shown in Supplementary Fig. S1, AMKP exhibited no cytotoxicity at concentrations up to 3200 μg/mL.

2.6.1 AMKP dose-gradient treatment assay

Cells were divided into five groups: Control (Con), Model (LPS), low-dose AMKP treatment (LPS+PL), medium-dose AMKP treatment (LPS+PM), and high-dose AMKP treatment (LPS+PH). Except for the Control group, all other groups were treated with 1 μg/mL LPS for 24 h to establish the cellular LPS model [17]. Subsequently, the AMKP treatment groups were administered with 100, 200, and 400 μg/mL of AMKP, respectively, and treated for an additional 24 h [18]. The Control and Model groups received an equal volume of culture medium.

2.6.2 Intervention assay with the autophagy inhibitor 3-MA

Cells were divided into five groups: Control (Con), Model (LPS), AMKP treatment (LPS+P), autophagy inhibition (LPS+3-MA), and autophagy inhibition combined with treatment (LPS+3-MA+P). Except for the Control group, all other groups were treated with 1 μg/mL LPS for 24 h to establish the cellular LPS model. Subsequently, the LPS+P group was treated with 400 μg/mL AMKP, the LPS+3-MA group was treated with 2.5 mM 3-MA, and the LPS+3-MA+P group was treated with both 400 μg/mL AMKP and 2.5 mM 3-MA, all for an additional 24 h. The Control and Model groups received an equal volume of culture medium.

2.6.3 Intervention assay with the ER stress activator TUN

Cells were divided into five groups: Control (Con), ER stress activation (TUN), AMKP treatment (TUN+P). Except for the Control group, all other groups were treated with 1 μg/mL TUN for 6 h to establish the cellular ER stress model. Subsequently, the TUN+P group continued to be treated with 400 μg/mL AMKP for an additional 18 h. The Con and TUN groups received an equal volume of culture medium at each corresponding stage.

2.7 RNA extraction and qPCR analysis

The methods for RNA extraction from tissue and cell samples and qPCR were consistent with those previously described [19]. The primer sequences are listed in Table S1.

2.8 Histopathology and immunofluorescence

Distal colon was collected and fixed in Carnoy's Fluid. After 24 h, replace it with 75% ethanol. Dehydrated and embedded in paraffin as previously described. Sections (4 μm) were obtained and stained with H&E and AB&PAS.

Colon paraffin sections were first deparaffinized in xylene and rehydrated through a graded ethanol series to water. Antigen retrieval was then performed using a EDTA antigen retrieval solution (pH 8.0; cat: C1036; Solarbio, Beijing, China) at 95–100 °C for 15 min. After cooling to room temperature, the sections were blocked with 5% bovine serum albumin (BSA) in PBS for 1 h at room temperature to prevent nonspecific binding. Subsequently, the sections were incubated with the primary antibody against MUC2 (cat: ab272692, 1:100; Abcam, UK) at 4 °C overnight. Following three washes with PBS containing 0.1% Tween-20 (PBST), the sections were incubated with an HRP-conjugated secondary antibody (cat: ab150077, 1:400; Abcam, UK) for 1 h at room temperature. Slides were mounted with a DAPI stain (cat: C0065; Solarbio, Beijing, China) and images were acquired using an Pannoramic MIDI microscope (3DHISTECH Ltd., Hungary).

2.9 Western blot

Protein extraction and western blot were performed as previously described [10]. The antibodies used were: Grp78 (Cat: 11587-1-AP), p62 (Cat: 18420-1-AP), Beclin1 (Cat: 11306-1-AP), GAPDH (Cat: 10494-1-AP), CHOP (Cat: 15204-1-AP) and LC3 (Cat: 14600-1-AP), were purchased from Proteintech Group, Inc. (Wuhan, China).

2.10 ELISA

Human Mucin 2 (MUC2) ELISA Research Kit was purchased from Jiangsu Meimian Industrial Co., Ltd (Jiangsu, China). After collecting the cell culture supernatant, perform the tests according to the instructions.

2.11 16S rRNA sequencing analysis

The method for DNA extraction and amplification from mouse fecal samples was performed as described in our previous study. Sequencing was conducted by Genepioneer Biotechnologies Co., Ltd. (Nanjing, China) using the Illumina MiSeq sequencing platform.

2.12 Statistical analysis

GraphPad Prism Software (V.10.0) was used for statistical analysis and the preparation of most figures. ImageJ (V.2.3.0) was employed to determine the positive signals in immunofluorescence and Western blot images. The statistical comparisons were assessed by one-way analysis (ANOVA) and unpaired t-test, as indicated in the figure legends.

3. Results

3.1 Extraction, Isolation, Purification and Preliminary Characterization of AMKP

As shown in Fig. 1A, crude AMKP was extracted using the water extraction and alcohol precipitation method, followed by purification and detection. Following ion-exchange chromatography of the crude AMKP, negligible peaks were observed in the AMKP-E2, AMKP-E3, and AMKP-E4 fractions. This indicates that the crude AMKP consisted predominantly of neutral polysaccharides. Consequently, the AMKP-E1 fraction was collected for subsequent purification (Fig. 1B). AMKP-E1 was then subjected to gel filtration column chromatography, yielding a single symmetrical peak elution curve as shown in Fig. 1C. The elution fractions in the 210–265 min region were collected. Repeated gel filtration column chromatography was performed to obtain purified AMKP. The molecular weight calibration curve is shown in Figs. S2A–C. HPGPC analysis revealed that AMKP exhibited a single, symmetrical peak, with Mw = 2.68 kDa, Mn = 2.026 kDa, and Mw/Mn = 1.32 (Fig. 1D and Table 1). Ion chromatography analysis revealed that AMKP is composed of glucose and fructose in a ratio of 9.73:90.27 (Fig. 1E).

Table 1 Molecular Weights of AMKP

Sample name	RT(min)	Mp（Da）	Mw（Da）	Mn（Da）	Mw/Mn
AMKP	42.115	2437	2680	2026	1.32

The structural characteristics of AMKP were analyzed using FT-IR. Infrared spectroscopy scanning was performed in the range of 4000–400 cm^{-1}, and the results are shown in Fig. 1F. The infrared spectrum exhibits typical features of polysaccharide substances [20]. As can be seen from the figure (Fig. 1F), the broad and strong absorption peak at 3370 cm^{-1} corresponds to the O–H stretching vibration of sugars. The smaller absorption peak at 2931 cm^{-1} is attributed to the C–H stretching vibration of methyl or methylene groups. The peaks between 1400 and 1200 cm^{-1} are likely due to the C–H bending vibrations of sugars. Based on the above, the sample can be identified as a polysaccharide substance. The peak at 1656 cm^{-1} is the absorption

peak of O–H bending vibration, which is a characteristic absorption peak indicating the binding of water molecules to the polysaccharide [20, 21]. The absorption peaks at 935 cm^{-1}, 874 cm^{-1}, and 818 cm^{-1} suggest the presence of stretching vibrations caused by β-fructofuranosyl units [20, 21]. The above FT-IR results confirm that AMKP is primarily composed of fructose in the β-furanose configuration. To further elucidate the glycosidic linkages of AMKP, polysaccharide methylation analysis was performed. The total ion chromatogram (TIC) of AMKP is shown in Fig. 1G, and the MS/MS spectra are presented in Fig. S3A–F. By comparing with literature data [22, 23] and the ion fragment mass spectra from the database of the Complex Carbohydrate Research Center at the University of Georgia (Fig. S3G), the results indicate that the glycosidic linkages of AMKP are primarily 1,2-Fru*f* (78.56%), t-Fru*f* (10.32%), and t-Glc*p* (9.72%) (Table 2).

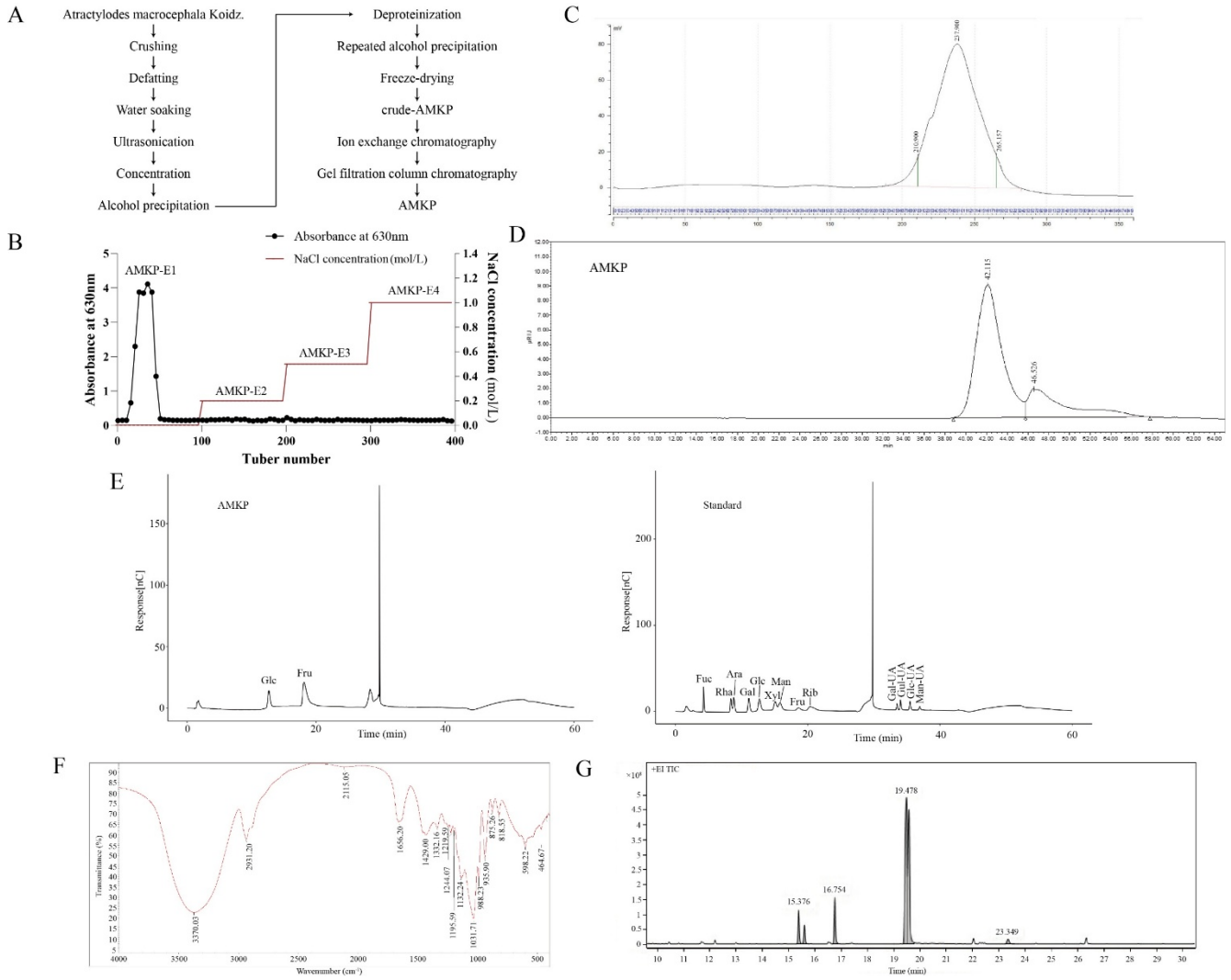


Figure 1. Extraction, Isolation, Purification and Preliminary Characterization of AMKP. (A) Extraction and isolation process of AMKP. (B) Elution profile of ion-exchange column chromatography of crude AMKP. (C) Elution profile of gel filtration column chromatography of AMKP-E1. (D) HPGPC chromatogram of AMKP (The peak at 46.526 min corresponded to the solvent front). (E) Ion chromatograms of AMKP and monosaccharide standards. (F) FT-IR spectrum of AMKP. (G) Total ion chromatogram of AMKP.

Table 2 Analysis of Glycosidic Linkages in AMKP

Linkages	Partially methylated alditol acetates (PMAAs)	MW	RT (min)	Peak area	Relative molar mass	Relative molar

						ratio(%)
t-Fru*f*	2,5-di-*O*-acetyl-1,3,4,6-tetra -*O*-methyl mannitol	323	15.376	383761533.9	1188116.204	6.645
t-Fru*f*	2,5-di-*O*-acetyl-1,3,4,6-tetra -*O*-methyl glucitol	323	15.596	212398969.8	657581.950	3.678
t-Glc*p*	1,5-di-*O*-acetyl-2,3,4,6-tetra -*O*-methyl glucitol	323	16.754	561322046.1	1737839.152	9.720
1,2-Fru*f*	1,2,5-tri-O-acetyl-3,4,6-tri-O-methyl mannitol	351	19.478	2785279637	7935269.622	44.383
1,2-Fru*f*	1,2,5-tri-O-acetyl-3,4,6-tri-O-methyl glucitol	351	19.579	2144992154	6111088.759	34.180
1,2,6-Fru*f*	1,2,5,6-tetra -O-acetyl-3,4-di-O-methyl-hexitol (mannitol, glucitol)	379	23.349	94428580.65	249151.928	1.394

3.2 NMR analysis

To further obtain structural characteristic information of AMKP, one-dimensional NMR (^{1}H-NMR, ^{13}C-NMR, DEPT-135) and two-dimensional NMR (COSY, HSQC, HMBC, NOESY) analyses were performed. The spectra are shown in Figs. 2A–H. The complete ^{1}H and ^{13}C chemical shifts of each major sugar residue were obtained, and the linkage sequence between the sugar residues was deduced.

The hydrogen signals of polysaccharides mostly appear in the range of δ 3.0–5.5 ppm. Typically, the resonance region of anomeric protons (H-1) lies between δ 4.0–5.5 ppm, where ^{1}H chemical shifts of α-sugars are generally greater than 4.95 ppm, while those less than 4.95 ppm indicate β-sugars [24]. In the ^{1}H-NMR spectrum of the polysaccharide sample (Fig. 2A), no distinct strong anomeric hydrogen (H-1) signals were observed in the region of δ 4.2–5.5 ppm. The other hydrogen signals were concentrated in the region of δ 3.0–4.5 ppm, with severe signal overlap, making them difficult to assign.

Compared to the ^{1}H-NMR spectrum, the ^{13}C-NMR spectrum of the polysaccharide sample (Fig. 2C) exhibits fewer spectral lines. Multiple anomeric carbons are present in the δ 90–110 ppm anomeric carbon region, with strong, distinct signals notably in the δ 103–105 ppm region. However, comparative analysis of the ^{13}C-NMR and DEPT-135 spectra revealed that the peaks in the δ 103–105 ppm anomeric carbon region disappeared in the DEPT-135 spectrum (Fig. 2D). Furthermore, no correlation peaks were observed in this anomeric region in the HSQC spectrum (Fig. 2E), indicating the absence of directly attached protons to these anomeric carbons. This suggests these signals belong to quaternary carbons, implying the sample contains a significant amount of ketose sugars. Combining this with the monosaccharide composition and methylation analysis results, which showed fructose as the most abundant sugar, these anomeric carbon signals are consistent with the NMR characteristics of fructose residues. The signals in this region are thus assigned to the anomeric carbons (C-2) of fructofuranosyl residues. The major signal peaks at δ 103.18 ppm and δ 103.63 ppm indicate that the fructose residues are exclusively in the β-configuration, suggesting the presence of two distinct types of fructose residues. Based on literature reports [21, 25] and the methylation analysis results, these are respectively assigned to the C-2 signals of →1)-β-D-Fruf-(2→ and β-D-Fruf-(2→, labeled as fructose residues Fru1,2 and Fru2. Methylation analysis indicated a minor amount of →1,6)-β-D-Fruf-(2→ residue;

however, based on literature data [26, 27], no corresponding signals for this residue were detected, likely due to its very low content (1.394%), which is below the detection limit of NMR.

In the DEPT-135 spectrum, distinct negative signals are observed in the δ 60–65 ppm region, consistent with the signal characteristics for C-1 and C-6 of fructose residues, thus tentatively assigned to the C-1 and C-6 signal region of fructose residues. Five sets of relatively distinct signal groups are present in the ^{13}C-NMR, DEPT-135, and HSQC spectra at approximately δ 80–82 ppm, δ 76–78 ppm, δ 73–74.5 ppm, δ 61–63 ppm, and δ 60–61 ppm. Based on literature reports [28, 29], these are assigned to the C-5, C-3, C-4, C-6, and C-1 signals of fructose residues, respectively. Strong correlation peaks for the characteristic fructose H-5/C-5 are present in the HSQC spectrum (δ 3.76/81.01 ppm). Combined with methylation results and literature references, the H-5/C-5 correlation at δ 3.77/81.01 ppm is assigned to both →1)-β-D-Fruf-(2→ and β-D-Fruf-(2→, labeled as Fru1,2 and Fru2, respectively.

Taking →1)-β-D-Fruf-(2→ (Fru1,2) as an example: Since no anomeric proton signal is present in the fructan's ^{1}H-NMR spectrum, its H-5 chemical shift is first determined as δ 3.76 ppm from the HSQC spectrum. Subsequently, using correlation peaks in the COSY spectrum (Fig. 2F) — Fru1,2 H-4/H-5 (δ 4.00/3.76 ppm), H-3/H-4 (δ 4.15/4.00 ppm), and H-5/H-6a, H-5/H-6b — the signals for H-4, H-3, and H-6a/6b are deduced as δ 4.00 ppm, δ 4.15 ppm, and δ 3.67/3.75 ppm, respectively. As its C-2 (δ 103.18 ppm) lacks an attached proton, the HMBC spectrum is utilized. A strong absorption peak for H-3/C-1 (δ 4.15/60.61 ppm) allows the deduction of the C-1 chemical shift as δ 60.61 ppm. Corresponding HSQC correlation peaks at δ 3.62/60.61 ppm and δ 3.82/60.61 ppm then provide the H-1a/1b signals as δ 3.62/3.82 ppm. Through the HSQC correlations, the chemical shifts for C-1, C-2, C-3, C-4, C-5, and C-6 are assigned as δ 60.61 ppm, δ 103.18 ppm, δ 76.92 ppm, δ 74.21 ppm, δ 81.01 ppm, and δ 62.07 ppm, respectively. Following a similar methodology, the ^{1}H and ^{13}C signals for the fructose residue β-D-Fruf-(2→ (Fru2) are deduced. The detailed chemical shift assignments are summarized in Table 3.

Table 3 Chemical Shift Assignments of ^{1}H and ^{13}C for Sugar Residues in AMKP

Sugar Residues			**Chemical Shift（ppm）**					
			1	**2**	**3**	**4**	**5**	**6**
Fru$_{1,2}$	→1)-β-D-Fru*f*-(2→	**H**	3.62/3.82		4.15	4.00	3.76	3.67/3.75
		C	60.61	103.18	76.92	74.21	81.01	62.07
Fru$_2$	β-D-Fru*f*-(2→	**H**	3.62/3.82		4.14	4.00	3.76	3.67/3.75
		C	60.64	103.63	77.45	74.21	81.01	62.07
G$_t$	α-D-Glc*p*-(1→	**H**	5.34	3.46	3.67	3.37	3.75	3.67/3.72
		C	92.42	71.02	72.39	69.15	72.34	60.41

In the HSQC spectrum, a correlation peak is observed for the anomeric signals at δ 5.34 ppm (H-1) and δ 92.42 ppm (C-1). This anomeric signal is assigned to the terminal proton signal of α-Glcp. Subsequently, the H-2, H-3, H-4, H-5, and H-6a/6b signals of this sugar residue were deduced via correlation peaks in the COSY spectrum. The chemical shifts for H-2, H-3, H-4, H-5, and H-6a/6b of this residue are assigned as δ 3.46 ppm, δ 3.67 ppm, δ 3.38 ppm, δ 3.75 ppm, and δ 3.67/3.72 ppm, respectively. After assigning the chemical shifts of the protons on the sugar ring, the corresponding carbon chemical shifts (C-1 to C-6) were assigned via the HSQC correlation spectrum as δ 92.42 ppm, δ 71.02 ppm, δ 72.39 ppm, δ 69.15 ppm, δ 72.34 ppm, and δ

60.41 ppm, respectively. Combined with methylation analysis results and literature reports [21, 30, 31], this sugar residue is inferred to be α-D-Glcp-(1→, labeled as Gt. Its chemical shift assignments are listed in Table 3.

The linkage sequence between sugar residues was further deduced using HMBC and NOESY spectra. The long-range couplings in HMBC spectra—between the anomeric proton of one residue and carbons of other residues, or between the anomeric carbon of one residue and protons of other residues—along with strong NOE signals between protons at the linkage sites of adjacent residues (due to spatial proximity), were utilized. As shown in the HMBC (Fig. 2G) and NOESY (Fig. 2H) spectra of AMKP, the following key correlations were identified: (1) In the HMBC spectrum, a correlation peak was observed between the anomeric proton H-1 (δ 5.34 ppm) of residue Gt and the anomeric carbon C-2 (δ 103.18 ppm) of residue Fru1,2 (correlation: Gt H-1 / Fru1,2 C-2), indicating a →1)-β-D-Fruf-(2→1)-α-D-Glcp linkage. (2) In the HMBC spectrum, a correlation was found between protons H-1 (δ 3.62/3.82 ppm) of residue Fru1,2 and its own anomeric carbon C-2 (δ 103.18 ppm) (correlation: Fru1,2 H-1 / Fru1,2 C-2), indicating a →1)-β-D-Fruf-(2→1)-β-D-Fruf-(2→ linkage. (3) In the HMBC spectrum, a correlation was observed between H-1 (δ 3.62/3.82 ppm) of residue Fru1,2 and C-2 (δ 103.63 ppm) of residue Fru2 (correlation: Fru1,2 H-1 / Fru2 C-2), indicating a β-D-Fruf-(2→1)-β-D-Fruf-(2→ linkage.

Based on the methylation analysis results, the molar ratio of the sugar residues →1)-β-D-Fruf-(2→, β-D-Fruf-(2→, t-Glcp, and →1,6)-Fruf-(2→ is 78.563:10.323:9.720:1.394 ≈ 56:7:7:1. For relative quantification using ^{1}H-NMR, referring to the NMR-based glucose and fructose ratio calculation methods described in the literature [32, 33], the integral values of the H-3 signal from the Fruf residue and the anomeric H-1 signal from the Glc-p residue in the ^{1}H spectrum (Fig. 2B) were used. The resulting hydrogen integral ratio of the sugar residues is $I_{(\text{Fruf H-3})} : I_{(\text{Glcp H-1})} = 22.78:1 \approx 23:1$. This differs from the corresponding molar ratio of Fru-f to Glc-p residues ((78.563+10.323):9.720 ≈ 9:1) obtained from methylation analysis. This discrepancy is likely because the polysaccharide sample primarily consists of fructose and glucose, and fructose is more susceptible to degradation under the high-temperature acidic hydrolysis conditions used, making accurate content determination challenging [27, 34]. Given the molecular weight determination results for AMKP, with Mp and Mw values of 2437 Da and 2680 Da respectively, it is inferred that the polysaccharide is a fructan with a backbone primarily composed of →1)-β-D-Fruf-(2→ residues, and only a small portion of the chains possess side chains connected at the O-6 position.

Based on the comprehensive analysis of monosaccharide composition determination, methylation analysis results, and one- and two-dimensional NMR information, the structure of AMKP is preliminarily deduced to be a fructan with a backbone primarily composed of →1)-β-D-Fruf-(2→ linkages. Its possible structural model is shown in Fig. 2I.

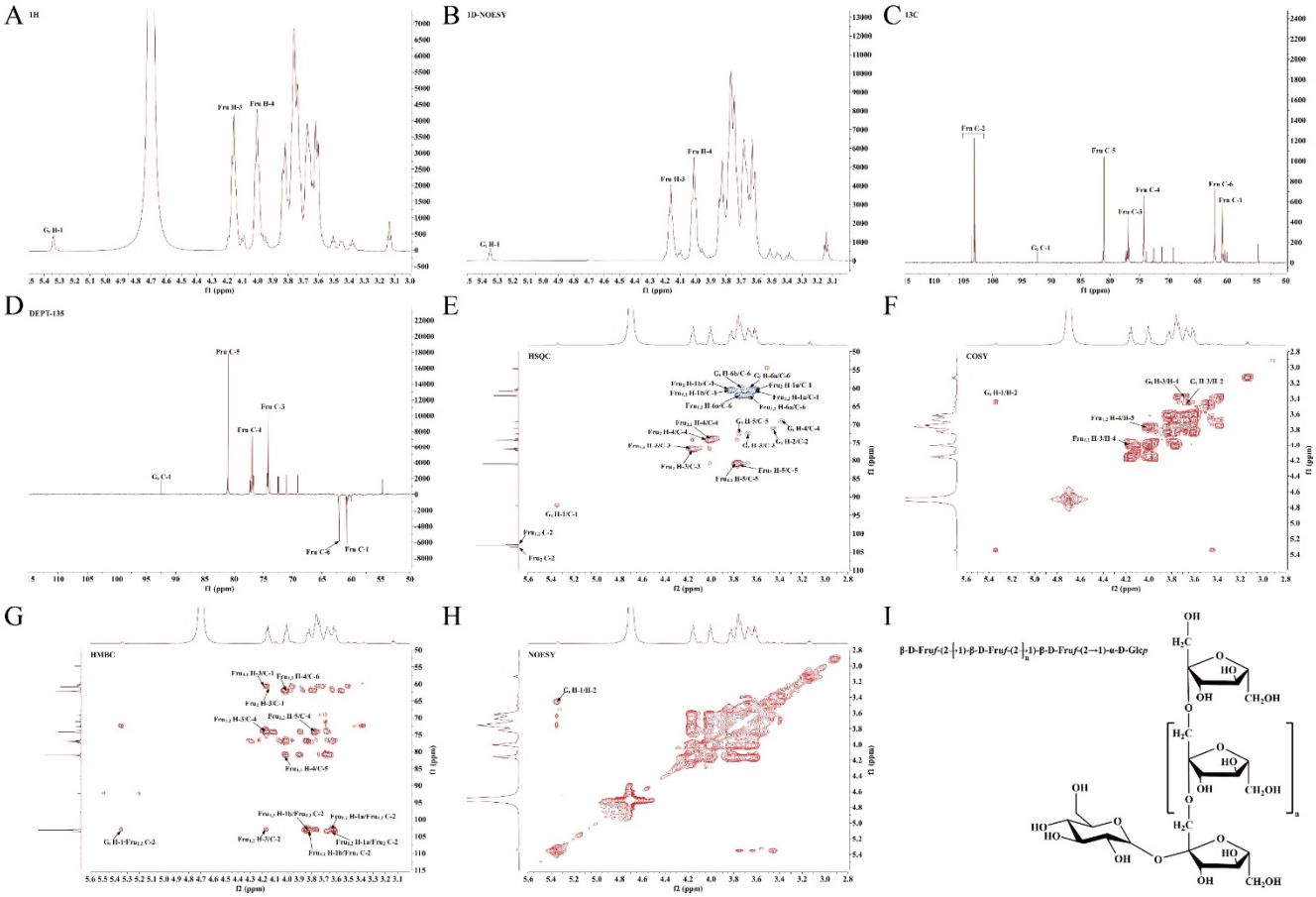


Figure 2. Structural characterization of AMKP. NMR spectra of AMKP, (A) ^{1}H NMR, (B) ^{1}D-NOESY NMR, (C) ^{13}C NMR, (D) DEPT-135, (E) HSQC, (F) COSY, (G) HMBC, (H) NOESY. (I) The putative structure of AMKP.

3.3 AMKP alleviates colitis in mice

To evaluate the therapeutic effects of AMKP on colitis in mice, we established a DSS-induced colitis model (Fig. 3A). The results showed that medium- and high-dose AMKP significantly alleviated body weight loss, colon shortening, and splenomegaly in mice. Moreover, high-dose AMKP notably reduced the disease activity index (DAI) score (Fig. 3B–E). Colonic mRNA detection revealed that all three doses of AMKP significantly decreased the DSS-induced upregulation of inflammatory factors (Fig. 3F–I). Pathological results indicated that AMKP attenuated inflammatory cell infiltration, goblet cell loss, and reduction of the mucus layer (Fig. 3J–K). Notably, AMKP increased the expression of MUC2 in the colon (Fig. 3L). These results indicate that AMKP exerts a dose-dependent alleviation effect on the colitis of mice.

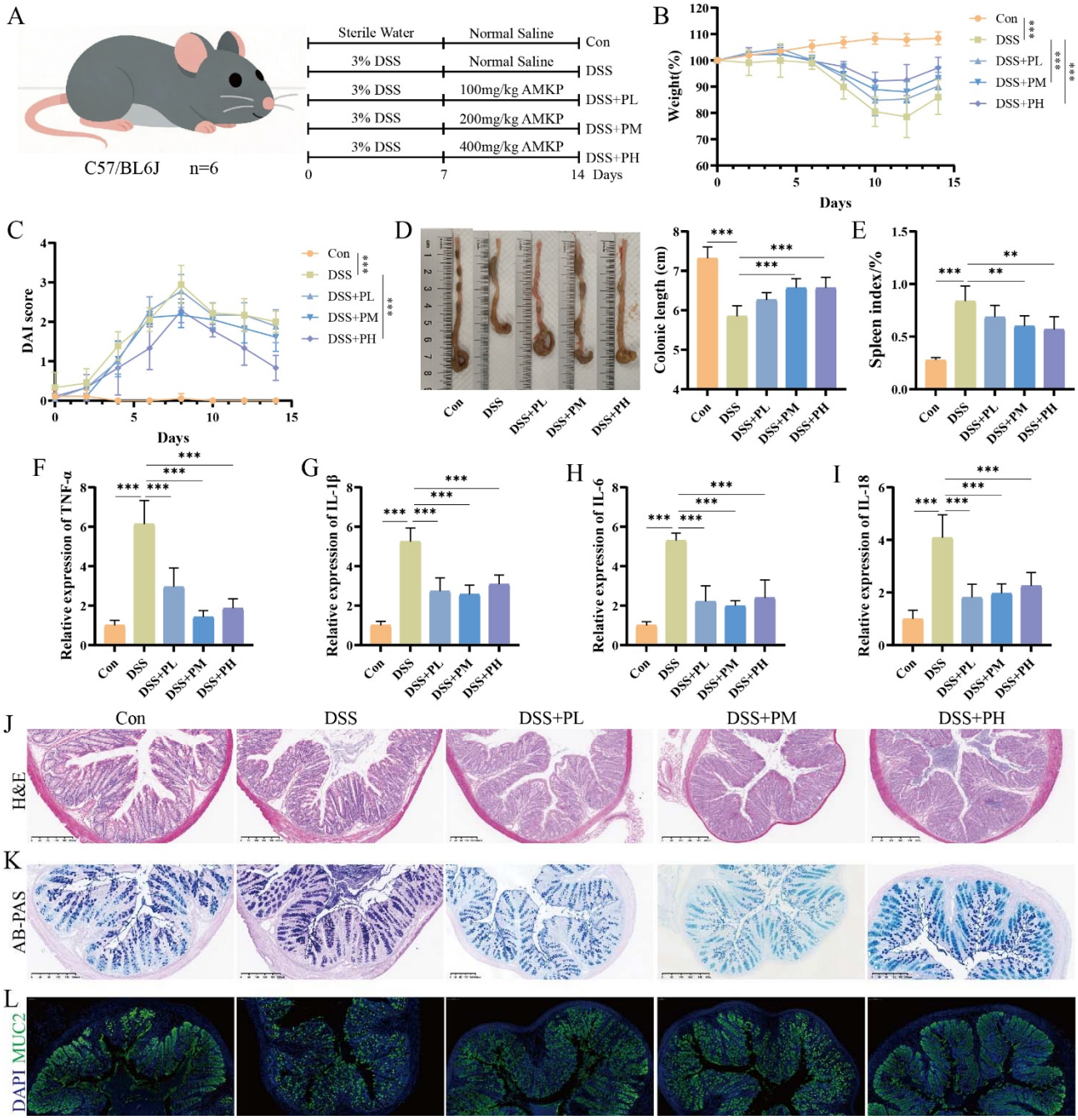


Figure 3 AMKP alleviates mouse colitis in a dose-dependent manner. (A) Animal experimental design. (B) Chart of weight change. (C) DAI score. (D) Representative colon pictures and chart of colon length. (E) Spleen index. Relative mRNA expression level (F) TNF-α, (G) IL-1β, (H) IL-6, (I) IL-18. Data represent mean ± SD (n = 6) and analyzed by one-way ANOVA with Tukey's multiple comparisons. ** and *** indicate $P < 0.01$ and $P < 0.001$. Representative images of sections of mouse colon tissue, (J) H&E, (K) AB-PAS. (L) Representative images of immunofluorescence sections of mouse colon tissue.

3.4 AMKP enhances autophagy and alleviates ER stress in the mouse intestine

To further investigate how AMKP alleviates colitis in mice, we examined colonic tissues and found that AMKP increased the mRNA expression of MUC2, Klf4, and glycosylation-related genes (C1galt1, C2gnt, C2GnT3) (Fig. 4A–E), which helps maintain MUC2 stability and glycosylation. Additionally, AMKP upregulated the expression of LC3 and Beclin1, while downregulating CHOP and Grp78 (Fig. 4F–I). At the protein level, AMKP similarly increased the expression of LC3 and Beclin1, and reduced the levels of Grp78,

p62, and CHOP (Fig. 4J–O). These results indicate that AMKP enhances autophagy, alleviates ER stress, and promotes MUC2 expression in the colon of mice with colitis.

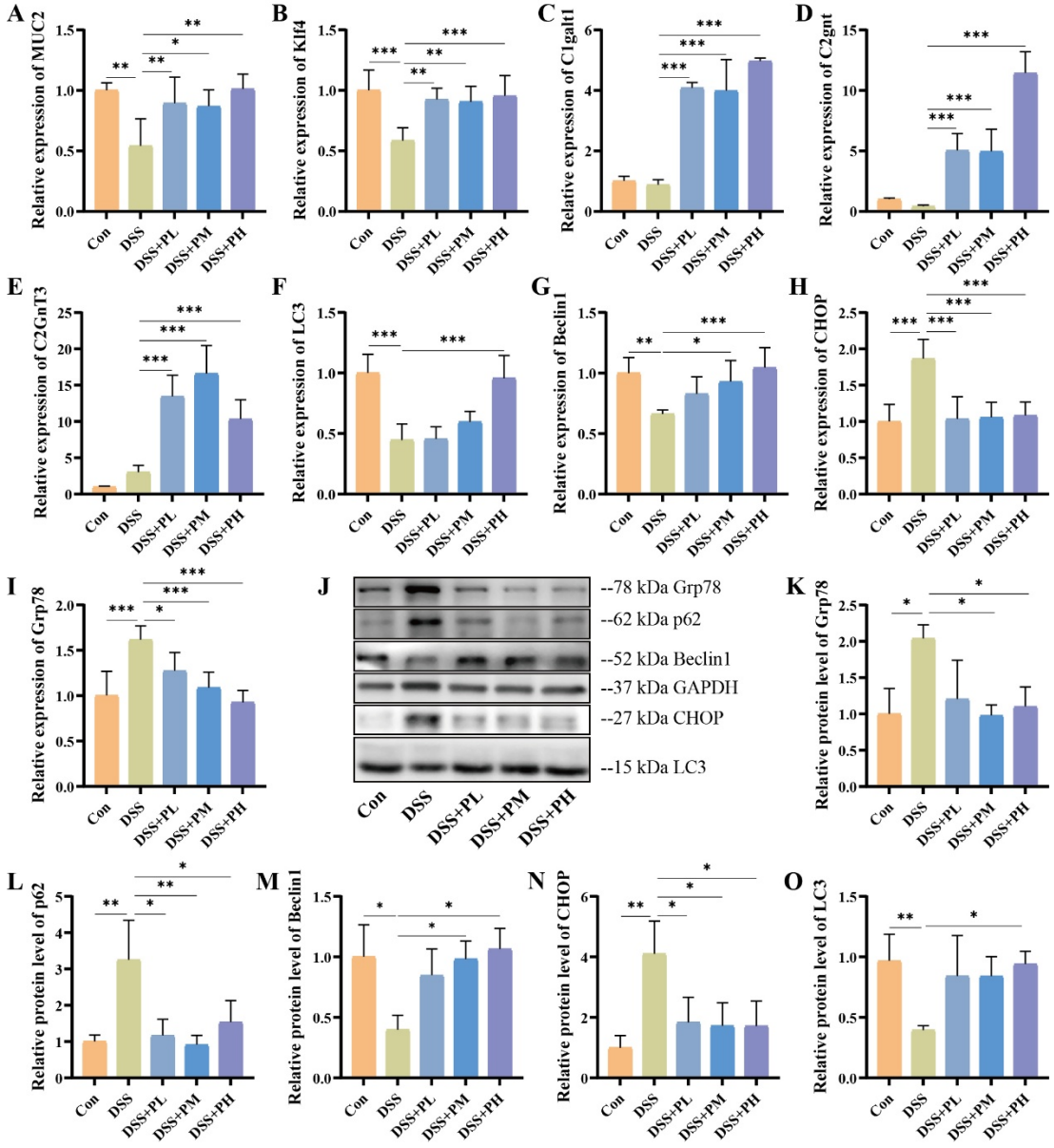


Figure 4. Effects of AMKP on intestinal MUC2, autophagy, and ER stress in mice. Relative mRNA expression level (A) MUC2, (B) Klf4, (C) C1galt1, (D) C2gnt, (E) C2GnT3, (F) LC3, (G) Beclin1, (H) CHOP, (I) Grp78. (J) Representative Western blot bands. Relative protein expression (K) Grp78, (L) p62, (M) Beclin1, (N) CHOP, (O) LC3. Data represent mean ± SD (A-I, n = 6; K-O, n = 3) and analyzed by one-way ANOVA with Tukey's multiple comparisons. *, ** and *** indicate $P < 0.05$, $P < 0.01$ and $P < 0.001$.

3.5 AMKP alleviates colitis by increasing MUC2 expression, independent of gut microbiota

It has been reported that many polysaccharides exert therapeutic effects by modulating the gut microbiota. To investigate whether the action of AMKP depends on gut microbes, we administered ABX via oral gavage to deplete the gut microbiota in mice. After ABX administration, fecal samples were collected for 16S sequencing. The results showed that compared with the Con group, the ABX group exhibited no significant changes in the Chao1 index or Shannon index (Fig. S4A-B). At the phylum and genus levels, the abundance of dominant microbes observed in the Con group was significantly reduced in the ABX group (Fig. S4C-D). Beta-diversity analysis revealed a significant alteration in the gut microbial structure of the ABX

group (Fig. S4E-F). These results indicate that the gut microbiota of mice was significantly disrupted, and subsequent experiments were continued as outlined in Fig. 5A.

Results from animal experiments showed that even when the gut microbiota was significantly disrupted, AMKP still alleviated DSS-induced body weight loss, increased diarrhea, colon shortening, and spleen enlargement (Fig. 5B-E). At the molecular level, the mRNA expression of colonic inflammatory cytokines (TNF-α, IL-1β, IL-6 and IL-18) was significantly reduced (Fig. 5F-I). Histological examination revealed that AMKP reduced inflammatory infiltration and goblet cell loss in the colon (Fig. 5J-K), and increased the expression of MUC2 (Fig. 5L). These results indicate that the alleviation of colitis by AMKP, mediated through increased MUC2 expression, is independent of gut microbes.

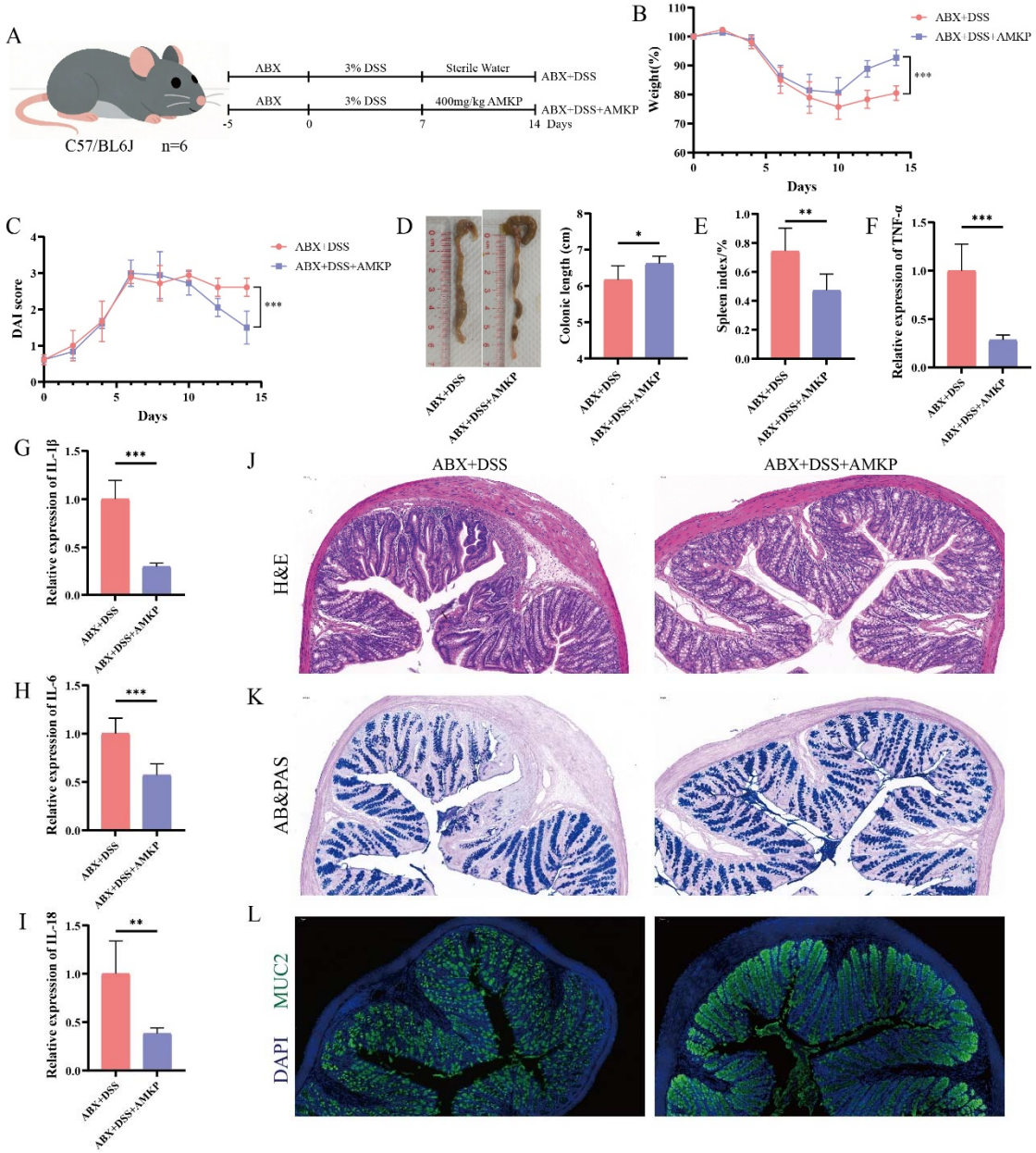


Figure 5. The therapeutic effect of AMKP is independent of gut microbiota. AMKP alleviates mouse colitis in a dose-dependent manner. (A) Animal experimental design. (B) Chart of weight change. (C) DAI score. (D) Representative colon pictures and chart of colon length. (E) Spleen index. Relative mRNA expression level (F) TNF-α, (G) IL-1β, (H) IL-6, (I) IL-18. Data represent mean ± SD (n = 6) and analyzed by unpair t-test. *, ** and *** indicate $P < 0.05$, $P < 0.01$ and $P < 0.001$. Representative images of sections of mouse colon tissue, (J) H&E, (K) AB-PAS. (L) Representative images of immunofluorescence sections of mouse colon tissue.

3.6 AMKP activation induces autophagy in the colon of ABX-pretreated mice, alleviating ER stress

To determine whether the effects of AMKP on the mouse colon are influenced by ABX pretreatment, we examined the expression of factors associated with MUC2, autophagy and ER stress in the colon. Results showed that AMKP significantly upregulated the mRNA expression of MIC2, Klf4, C1galt1, C2GnT, and C2gnt3 in the mouse colon (Fig. 6A-E). Similarly, AMKP increased the mRNA and protein levels of LC3 and Beclin1, while decreasing the expression of CHOP, Grp78 (at both mRNA and protein levels), and p62 protein (Fig. 6F-O). These findings were consistent with those observed in the absence of ABX pretreatment, indicating that AMKP activates colonic autophagy, alleviates ER stress, and enhances MUC2 expression through a microbiota-independent mechanism.

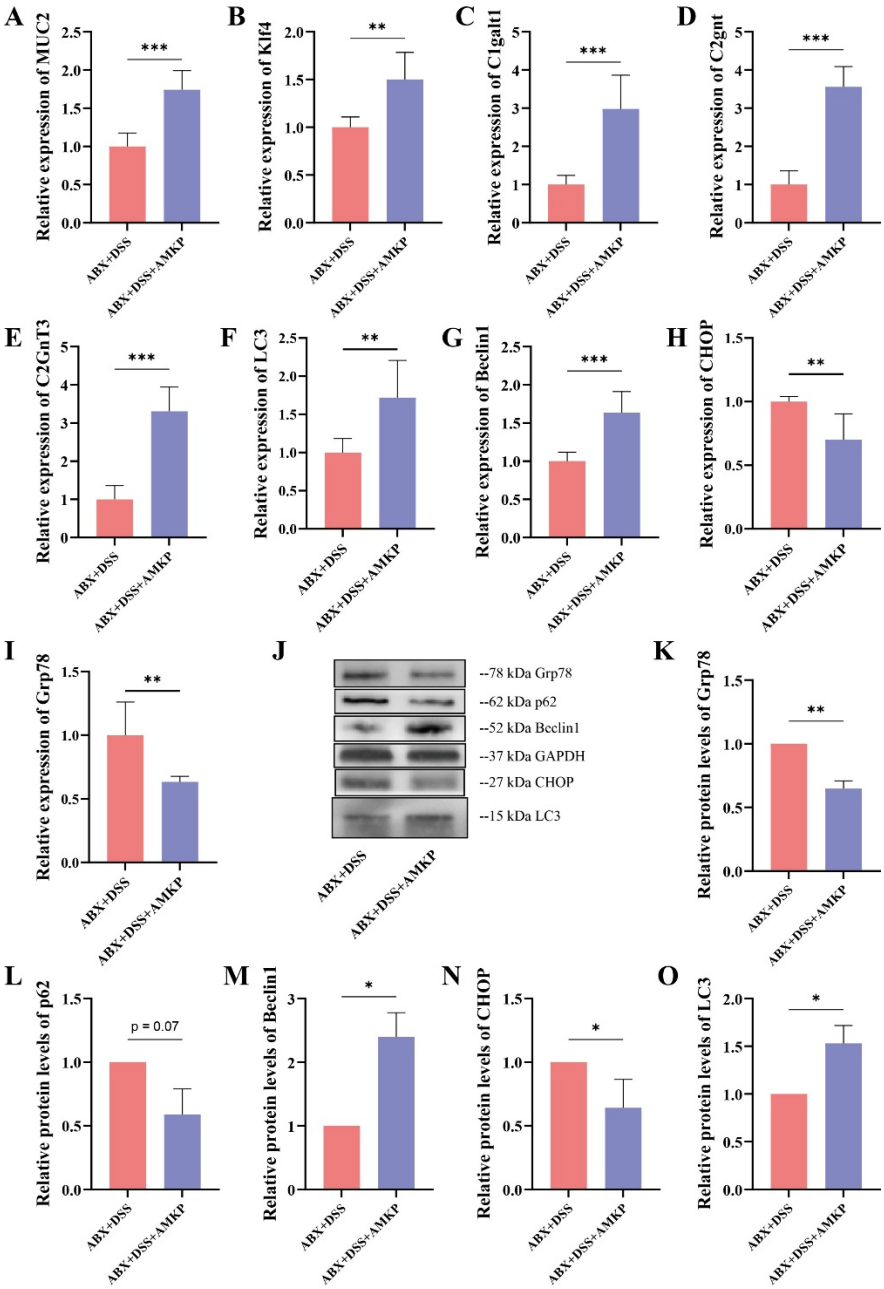


Figure 6. AMKP activation induces autophagy in the colon of ABX-pretreated mice, alleviating ER stress. Relative mRNA expression level (A) MUC2, (B) Klf4, (C) C1galt1, (D) C2gnt, (E) C2GnT3, (F) LC3, (G) Beclin1, (H) CHOP, (I) Grp78. (J) Representative Western blot bands. Relative protein expression (K) Grp78, (L) p62, (M) Beclin1, (N) CHOP, (O) LC3. Data represent mean ± SD (A-I, n = 6; K-O, n = 3) and analyzed by one-way ANOVA with Tukey's multiple comparisons. *, ** and *** indicate $P < 0.05$, $P < 0.01$ and $P < 0.001$.

3.7 AMKP alleviates mouse colitis in an autophagy-dependent manner

To determine whether autophagy is essential for the therapeutic action of AMKP, we administered 3-MA (10 mg/kg, *i.p.*) to DSS-challenged mice to pharmacologically inhibit autophagy (Fig. 7A). In contrast to the DSS + AMKP group, 3-MA administration markedly delayed the restoration of body weight and DAI scores, and exacerbated pathological manifestations including colonic atrophy and splenomegaly (Fig. 7B-E). Following 3-MA treatment, the mRNA expression of pro-inflammatory cytokines (TNF-α, IL-1β, IL-6, and IL-18) was significantly upregulated in the colon (Fig. 7F-I). Histologically, colons from 3-MA-treated mice exhibited exacerbated inflammatory infiltration, goblet cell loss, and reduced MUC2 expression (Fig. 7J-L). These results indicate that 3-MA treatment completely abolished the therapeutic effects of AMKP on colitis.

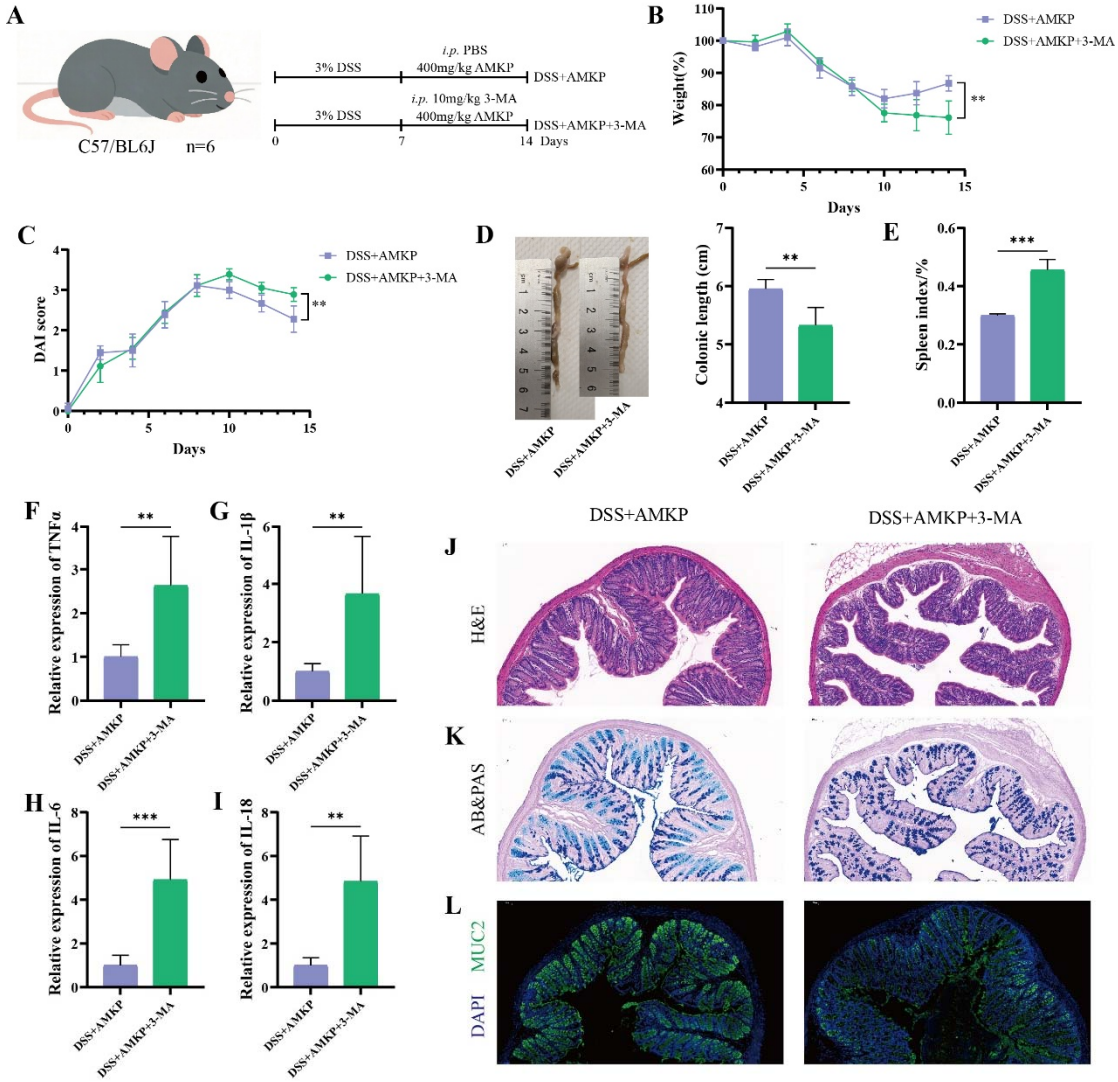


Figure 7. AMKP alleviates mouse colitis in an autophagy-dependent manner. (A) Animal experimental design. (B) Chart of weight change. (C) DAI score. (D) Representative colon pictures and chart of colon length. (E) Spleen index. Relative mRNA expression level (F) TNF-α, (G) IL-1β, (H) IL-6, (I) IL-18. Data represent mean ± SD (n = 6) and analyzed by unpair t-test. *, ** and *** indicate $P < 0.05$, $P < 0.01$ and $P < 0.001$. Representative images of sections of mouse colon tissue, (J) H&E, (K) AB-PAS. (L) Representative images of immunofluorescence sections of mouse colon tissue.

3.8 AMKP alleviates ER stress and upregulates MUC2 expression in an autophagy-dependent manner

Subsequently, we examined the expression of MUC2 and markers related to autophagy and ER stress in the mouse colon. Results showed that 3-MA treatment significantly downregulated the mRNA expression of

MUC2, Klf4, and C1galt1 in the mouse colon, but had no significant effect on the mRNA levels of C2gnt and C2GnT3 (Fig. 8A-E). Concurrent with this, 3-MA markedly reduced both the mRNA and protein levels of LC3 and Beclin1, while elevating the mRNA and protein expression of CHOP and Grp78 as well as the protein level of p62 (Fig. 8F-O). Collectively, these findings demonstrate that AMKP alleviates ER stress and upregulates MUC2 expression in an autophagy-dependent manner.

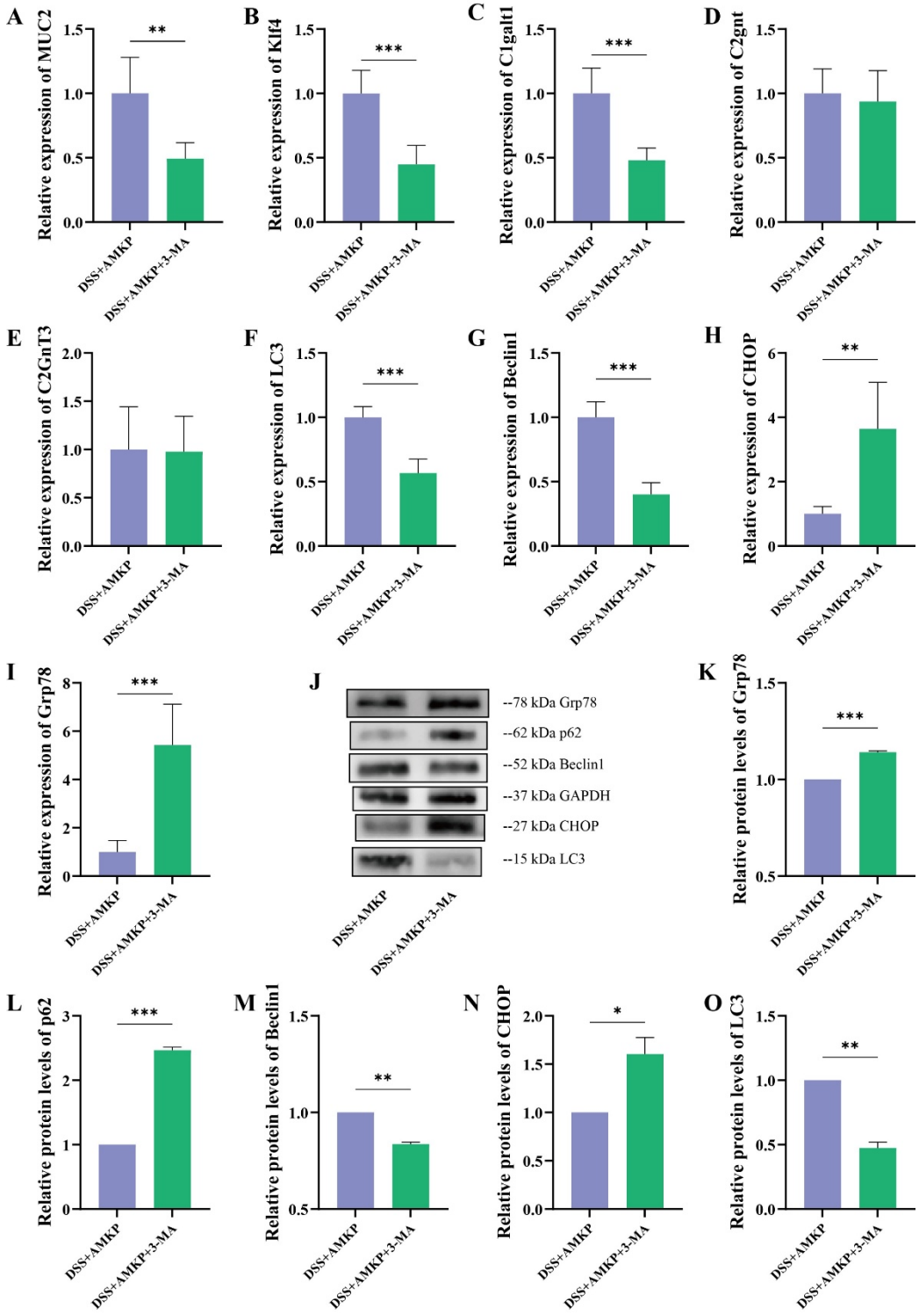


Figure 8. AMKP alleviates ER stress and upregulates MUC2 expression in an autophagy-dependent manner. Relative mRNA expression level (A) MUC2, (B) Klf4, (C) C1galt1, (D) C2gnt, (E) C2GnT3, (F) LC3, (G) Beclin1, (H) CHOP, (I) Grp78. (J) Representative Western blot bands. Relative protein expression (K) Grp78, (L) p62, (M) Beclin1, (N) CHOP, (O) LC3. Data represent mean ± SD (A-I, n = 6; K-O, n = 3) and analyzed by one-way ANOVA with Tukey's multiple comparisons. *, ** and *** indicate $P < 0.05$, $P < 0.01$ and $P < 0.001$.

3.9 AMKP increases MUC2 expression, enhances autophagy, and alleviates ER stress in LS174T cells

To assess whether AMKP can reach the intestine, we digested AMKP in artificial gastric and gastrointestinal fluids. The reducing sugar assay showed no significant change in concentration after simulated digestion (Fig. 9A), indicating that AMKP remained undigested. HPGPC analysis revealed no significant change in the molecular weight of AMKP before and after in vitro digestion (Fig.9B, Table 4), indicating that it can reach the colon intact to exert its bioactivity. We then induced an inflammatory state in LS174T cells using LPS, followed by stimulation with AMKP. The results demonstrated that AMKP significantly increased both the secretion of MUC2 into the culture medium and its mRNA expression (Fig. 9C–D). Consistent with the animal experiments, under inflammatory conditions, the mRNA levels of LC3 and Beclin1 decreased, while those of CHOP and Grp78 increased. AMKP treatment reversed these changes (Fig. 9E–H). At the protein level, AMKP similarly counteracted the LPS-induced upregulation of Grp78, p62, and CHOP, as well as the downregulation of LC3 and Beclin1 (Fig. 9I–N). These findings indicate that AMKP enhances MUC2 expression, promotes autophagy, and alleviates ER stress in LS174T cells.

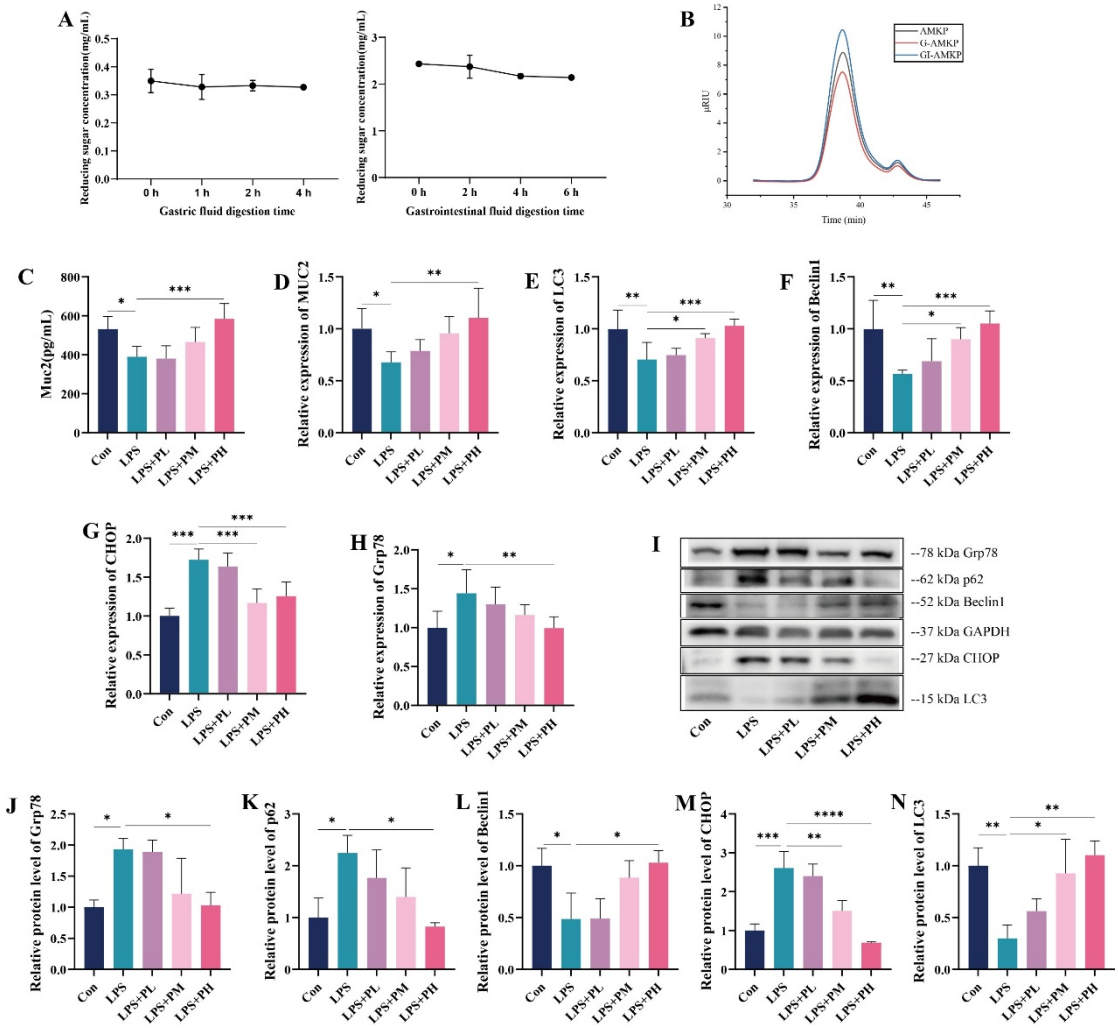


Figure 9. Effect of AMKP on MUC2 secretion in LS174T cells. Determination of reducing sugar content (n = 3), (A) gastric fluid digestion and gastrointestinal fluid digestion. (B) HPGPC analysis of AMKP, G-AMKP, GI-AMKP (The peak at 42.783 min corresponded to the solvent front). (C) MUC2 content in cell supernatant. Relative mRNA expression level, (D) MUC2, (E) LC3, (F) Beclin1, (G) CHOP, (H) Grp78. (I) Representative Western blot bands. Relative protein expression (K) Grp78, (L) p62, (M) Beclin1, (N) CHOP, (O) LC3. Data represent mean ± SD (C-H, n = 6; J-N, n = 3) and analyzed by one-way ANOVA with Tukey's multiple comparisons. *, ** and *** indicate $P < 0.05$, $P < 0.01$ and $P < 0.001$.

Table 4 Molecular Weights of AMKP, G-AMKP and GI-AMKP

Sample name	RT(min)	Mp（Da）	Mw（Da）	Mn（Da）	Mw/Mn
AMKP	38.703	2657	2844	1558	100
G-AMKP	38.673	2712	2896	1591	100
GI-AMKP	38.667	2722	2901	1583	100

3.10 AMKP-Promoted MUC2 Expression is Dependent on Autophagy

To investigate whether the promotion of MUC2 expression by AMKP is dependent on autophagy, we inhibited autophagy using 3-MA. After autophagy inhibition, both the secretion and mRNA expression of MUC2 were significantly reduced (Fig. 10A–B). When cells were treated with 3-MA, AMKP failed to increase the mRNA levels of LC3 and Beclin1 in LS174T cells (Fig. 10C–D). Moreover, autophagy inhibition elevated the mRNA expression of CHOP and Grp78, and these increases were not suppressed by AMKP treatment (Fig. 10E–F). At the protein level, 3-MA treatment reversed the effects of AMKP on upregulating LC3 and Beclin1 as well as downregulating Grp78, p62, and CHOP (Fig. 10G–L), consistent with the changes observed at the mRNA level. These results demonstrate that the AMKP-induced increase in MUC2 expression depends on the occurrence of autophagy.

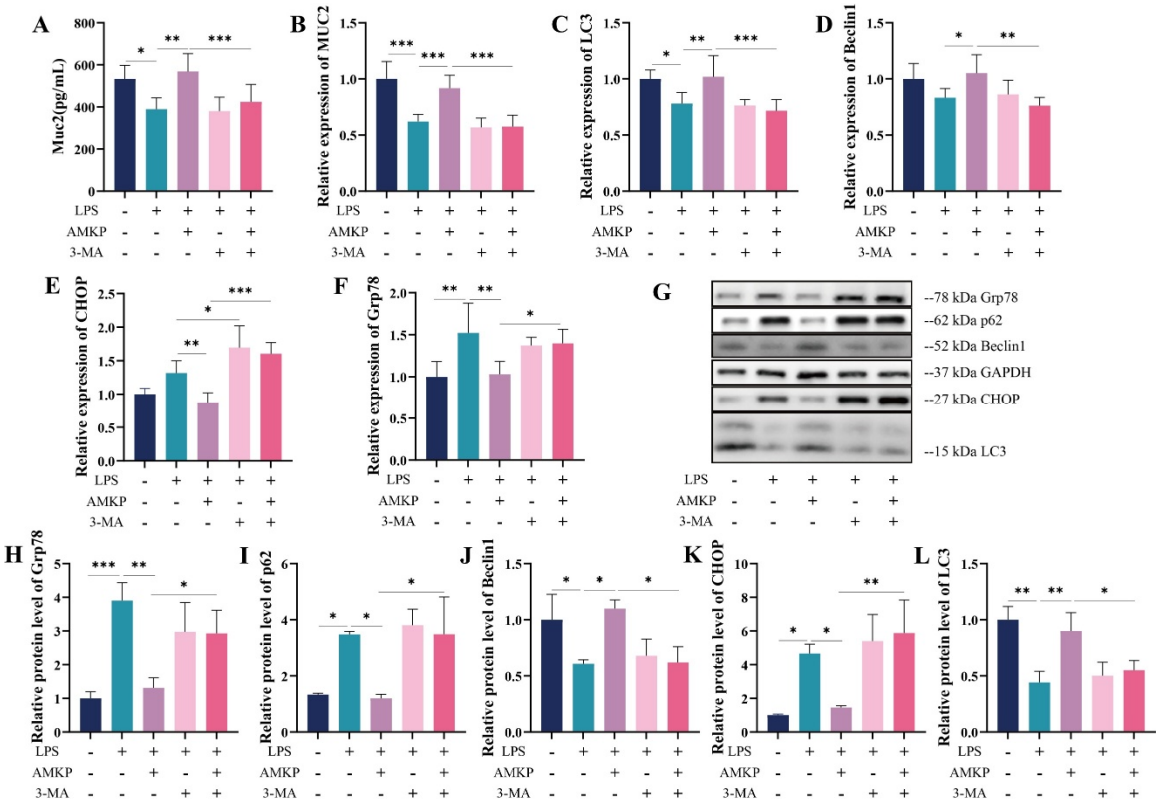


Figure 10. AMKP promotes MUC2 secretion in LS174T cells in an autophagy-dependent manner. (A) MUC2 content in cell supernatant. Relative mRNA expression level, (B) MUC2, (C) LC3, (D) Beclin1, (E) CHOP, (F) Grp78. (G) Representative Western blot bands. Relative protein expression (H) Grp78, (I) p62, (J) Beclin1, (K) CHOP, (L) LC3. Data represent mean ± SD (A-F, n = 6; H-L, n = 3) and analyzed by one-way ANOVA with Tukey's multiple comparisons. *, ** and *** indicate $P < 0.05$, $P < 0.01$ and $P < 0.001$.

3.11 AMKP Activates Autophagy Independently of ER Stress Induction

Since ER stress can activate autophagy while autophagy can conversely suppress ER stress, we used TUN to induce ER stress in LS174T cells to determine whether AMKP directly activates autophagy or acts

indirectly via ER stress. The results showed that upon induction of ER stress, both the secretion and mRNA expression of MUC2 were significantly inhibited (Fig. 11A–B). TUN treatment markedly increased the mRNA levels of LC3, Beclin1, CHOP, and Grp78. Notably, subsequent treatment with AMKP further elevated the expression of LC3 and Beclin1, while reducing the expression of CHOP and Grp78 (Fig. 11C–F). At the protein level, the expression trends of Grp78, Beclin1, CHOP, and LC3 were similar to those observed at the mRNA level. Correspondingly, TUN significantly increased p62 protein levels, an effect that was reversed by AMKP treatment (Fig. 11G–L). These findings indicate that AMKP directly activates autophagy rather than doing so indirectly through the induction of ER stress.

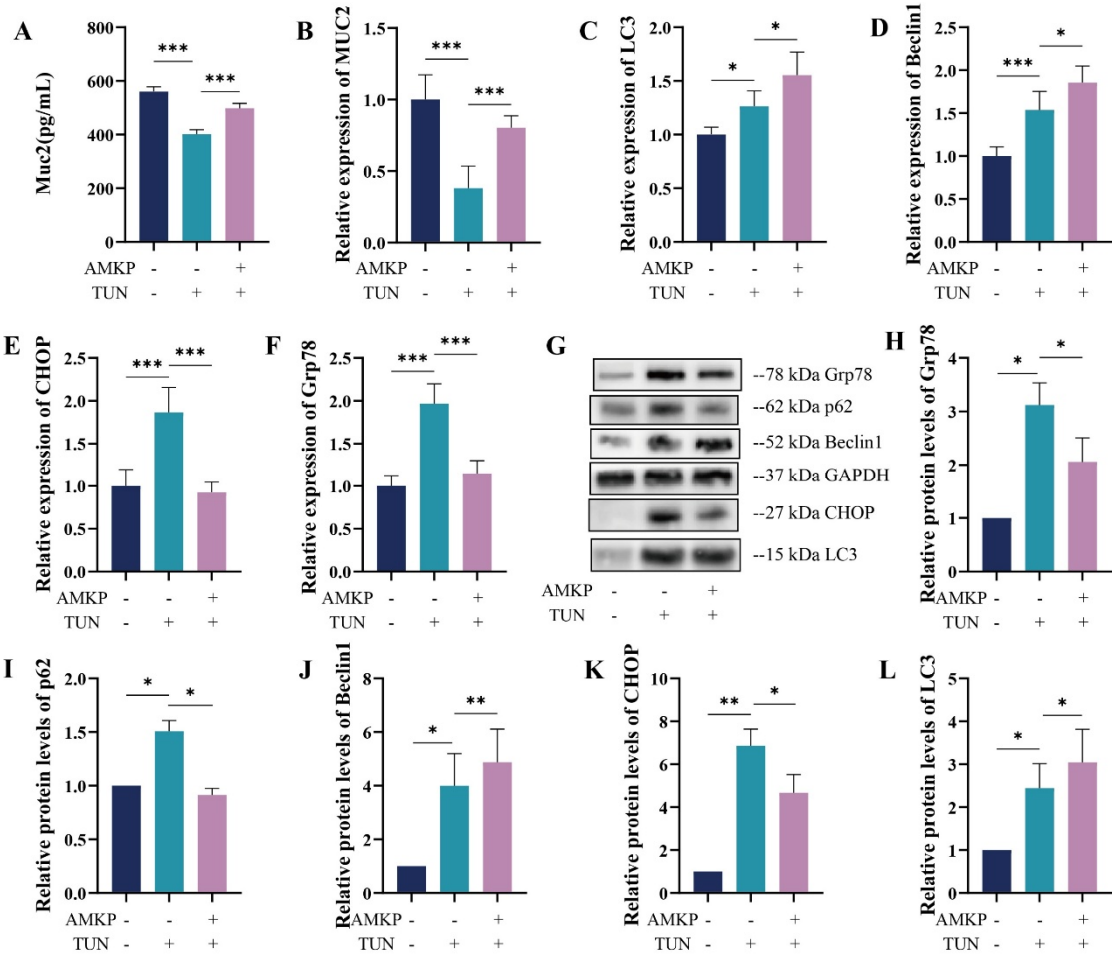


Figure 11. AMKP promotes MUC2 secretion in LS174T cells by activating autophagy independently of ER stress. (A) MUC2 content in cell supernatant. Relative mRNA expression level, (B) MUC2, (C) LC3, (D) Beclin1, (E) CHOP, (F) Grp78. (G) Representative Western blot bands. Relative protein expression (H) Grp78, (I) p62, (J) Beclin1, (K) CHOP, (L) LC3. Data represent mean ± SD (A-F, n = 6; H-L, n = 3) and analyzed by one-way ANOVA with Tukey's multiple comparisons. *, ** and *** indicate $P < 0.05$, $P < 0.01$ and $P < 0.001$.

4. Discussion

UC is characterized by chronic colonic inflammation and a disrupted mucus barrier, where depletion of the gel-forming mucin MUC2 drives bacterial translocation and sustained immunopathology [35]. Restoring MUC2 production via goblet cell modulation has thus emerged as a central therapeutic goal. In recent years, polysaccharides derived from medicinal-and-edible herbs have attracted considerable attention, as reflected by systematic reviews on *Panax ginseng* [36], *Tremella fuciformis* [37], and *edible fungi* [38]. However, most reported bioactive polysaccharides—including those from *Astragalus membranaceus*, *Artemisia argyi*, and

even previous *Atractylodes macrocephala*-exert their anti-colitis effects predominantly through gut microbiota remodeling [8, 9, 39, 40]. In contrast, the present study identifies AMKP, a low-molecular-weight (2.68 kDa) inulin-type fructan from *Atractylodes macrocephala Koidz.*, as a microbiota-independent regulator that directly targets intestinal goblet cells to activate autophagy and promote MUC2 secretion. This distinction represents a conceptual departure from the prevailing "polysaccharide-microbiota" paradigm and redefines the biological activity of AMKP.

Structurally, AMKP comprises a backbone of β-2,1-linked furanose fructose residues with minor terminal α-glucopyranose units, consistent with inulin-type fructans. Methylation analysis further detected trace 1,2,6-linked Fruf residues (1.394 mol%), although corresponding signals were absent in NMR spectra. This discrepancy likely reflects the extremely low abundance of this linkage, which falls below the detection threshold of NMR under our acquisition parameters—a well-documented limitation when minor glycosidic linkages coexist with dominant structural motifs. The overall low degree of polymerization (DP ≈ 16) differentiates AMKP from canonical inulins (DP 2–60 [41]) and underpins its notable resistance to simulated gastrointestinal digestion: AMKP showed no significant molecular weight reduction or reducing sugar release after gastric or duodenal incubation. Such acid and enzyme stability align closely with the "carrier adaptation–targeted modification–environmental response" framework recently proposed for food–medicine homologous active polysaccharides (F-MHAPs) [42]. Low-DP inulin-type fructans are increasingly recognized as being resistant to upper-GI enzymatic hydrolysis and capable of reaching the colon intact, where they either serve as fermentation substrates or, in the case of structurally defined small fructans, interact directly with epithelial sensors [43]. It has been reported that β2→1 fructans can activate TLR2 in T84 intestinal epithelial cells [44], suggesting that AMKP may also embody the latter—a shift from the classical "prebiotic fermentation" model of inulin to a "direct epithelial modulation" model, a transition also echoed in recent pectin- and fructan-based colonic protectants such as the active pectin from *Sanguisorba officinalis* roots [45].

Subsequently, we established a mouse colitis model using DSS. AMKP treatment alleviated the characteristic symptoms in a dose-dependent manner, including weight loss, aggravated diarrhea, colon shortening, and splenomegaly, while also mitigating histopathological damage. Notably, AMKP suppressed the expression of inflammatory factors and upregulated MUC2 expression. These therapeutic effects align with previously reported benefits of various plant-derived polysaccharides (such as *Portulaca oleracea L.* polysaccharide, *Polygonati kingianum* polysaccharide, polysaccharides from *Cistanche deserticola*) [5, 46, 47]. Critically, despite significant disruption of the microbial structure, these protective effects persisted following complete ABX treatment. We acknowledge that ABX treatment altered β-diversity and relative taxon abundance without significantly affecting α-diversity indices (Chao1, Shannon). This apparent discrepancy is biologically plausible: α-diversity reflects species richness and evenness within a sample, whereas β-diversity captures community composition across samples. Short-term, high-dose ABX regimens often reduce total bacterial load while leaving dominant taxa relatively stable, thereby preserving α-diversity but reshaping

β-diversity and relative abundances [48]. Our data therefore robustly support that AMKP's efficacy does not require an intact or diverse microbiota.

Mechanistically, AMKP directly acted on LS174T goblet cells to upregulate MUC2 transcription and protein secretion under inflammatory conditions. These effects were accompanied by increased LC3 and Beclin1 expression, alongside reduced levels of the ER stress markers Grp78, CHOP, and p62. Here, LC3 and Beclin1 serve as canonical autophagosome initiation and maturation markers, while Grp78 and CHOP indicate ER stress intensity; p62 acts as a selective autophagy substrate whose accumulation reflects impaired autophagic flux [49]. The observation that the autophagy inhibitor 3-MA completely abolished AMKP-induced MUC2 upregulation establishes autophagy as an essential mediator rather than a bystander [49, 50]. Importantly, AMKP's autophagy activation occurred independently of ER stress induction, as demonstrated by TUN experiments, suggesting that AMKP initiates autophagic flux through a direct epithelial signaling axis rather than secondary to ER perturbation. This mechanism contrasts sharply with microbiota-dependent polysaccharides, such as *A. argyi* polysaccharide, which ameliorates inflammation partly through flora-driven metabolic shifts [40], and expands upon recent insights into pectin-mediated mucosal protection [45].

Previous studies have demonstrated that β2→1-fructans protect barrier function by activating TLR2 in T84 cells [44], while *Dendrobium huoshanense* polysaccharides modulate lamina propria immune responses via TLR4 stimulation in intestinal epithelial cells [51]. Furthermore, enterocytes have been shown to internalize 1,3- and 1,4-linked polysaccharides through clathrin-mediated endocytosis [52]. In the present study, however, it remains unclear whether AMKP exerts its effects by activating specific receptors on goblet cells or via direct cellular uptake. Elucidating this distinction represents a critical direction for our future research.

5. Conclusion

In summary, we isolated, purified, and identified an inulin-type fructan with a molecular weight of 2.68 kDa from *Atractylodes macrocephala Koidz.*, and validated its effects in upregulating colonic MUC2 expression and alleviating colitis in mice. Notably, this therapeutic effect is achieved through AMKP acting directly on intestinal goblet cells in its intact molecular form, by activating autophagy and alleviating ER stress. This study expands the target of polysaccharides from the "microbial ecosystem" to "host epithelial cells themselves, particularly goblet cells," opening a new paradigm for understanding the immunomodulatory mechanisms of dietary fibers and herbal polysaccharides.

Conflict of Interest

The authors declare no conflict of interest.

Acknowledgements

All authors sincerely acknowledge the support provided by the National Natural Science Foundation of China (grants 32302913). All authors express sincere gratitude to Genepioneer Biotechnologies Co., Ltd. (Nanjing, China) for the technical support in 16S sequencing and to Wuhan Huashite Industrial Biotechnology Development Co., Ltd. (Wuhan, China) for the technical support in polysaccharide detection.

Reference

[1] C. Le Berre, S. Honap, L. Peyrin-Biroulet, Ulcerative colitis, Lancet. 402 (2023) 571-584. https://doi.org/10.1016/S0140-6736(23)00966-2.

[2] J.K. Gustafsson, G.C. Hansson, Immune Regulation of Goblet Cell and Mucus Functions in Health and Disease, Annu Rev Immunol. 43 (2025) 169-189. https://doi.org/10.1146/annurev-immunol-101721-065224.

[3] T. Breugelmans, B. Oosterlinck, W. Arras, et al., The role of mucins in gastrointestinal barrier function during health and disease, Lancet Gastroenterol Hepatol. 7 (2022) 455-471. https://doi.org/10.1016/S2468-1253(21)00431-3.

[4] T. Balasubramaniyam, H.-B. Ahn, J. Lim, et al., Therapeutic potential of polysaccharides in inflammation: current insights and future directions, International Immunopharmacology. 166 (2025) 115538. https://doi.org/10.1016/j.intimp.2025.115538.

[5] K. Ning, C. Shi, Y.-Y. Chi, et al., Portulaca oleracea L. polysaccharide alleviates dextran sulfate sodium-induced ulcerative colitis by regulating intestinal homeostasis, Int J Biol Macromol. 256 (2024) 128375. https://doi.org/10.1016/j.ijbiomac.2023.128375.

[6] S. La, M. Abaidullah, H. Li, et al., Alfalfa Polysaccharide Alleviates Colitis by Regulating Intestinal Microbiota and the Intestinal Barrier Against the TLR4/MyD88/NF-κB Pathway, Nutrients. 17(18) (2025) 3001. https://doi.org/10.3390/nu17183001.

[7] J.Y. Shi, Y.J. Wang, Q.W. Bao, et al., Polygonatum cyrtonema Hua polysaccharide alleviates ulcerative colitis via gut microbiota-independent modulation of inflammatory immune response, Carbohydr Polym. 356 (2025) 123387. https://doi.org/10.1016/j.carbpol.2025.123387.

[8] Q. Meng, M. Mao, C. Shentu, et al., Structural characterization of Atractylodes macrocephala polysaccharide 1 and its gut microbiota-mediated alleviation of ulcerative colitis, Carbohydr Polym. 377 (2026) 124863. https://doi.org/10.1016/j.carbpol.2025.124863.

[9] J. Wu, Q. Xu, Y. Yang, et al., A novel fructan from Atractylodes macrocephala ameliorates ulcerative colitis through gut microbiota-mediated PI3K/Akt signaling, Carbohydr Polym. 375 (2026) 124764. https://doi.org/10.1016/j.carbpol.2025.124764.

[10] W.J. Lv, Y.M. Ma, J.Y. Huang, et al., Polysaccharides derived from Shenling Baizhu San improve colitis via modulating tryptophan metabolism in mice, Int J Biol Macromol. 222 (2022) 1127-1136. https://doi.org/10.1016/j.ijbiomac.2022.09.246.

[11] M. Zhao, Y. Wang, R. Guan, et al., Paeoniae Radix Alba polysaccharides: Structural characterization, macrophage immunomodulation, and potent vaccine adjuvant activity, Carbohydr Polym. 380 (2026) 124883. https://doi.org/10.1016/j.carbpol.2025.124883.

[12] L. Jia, Y. Jiang, L. Wu, et al., Porphyromonas gingivalis aggravates colitis via a gut microbiota-linoleic acid metabolism-Th17/Treg cell balance axis, Nat Commun. 15 (2024) 1617. https://doi.org/10.1038/s41467-024-45473-y.

[13] Y. Wang, C. Li, J. Li, et al., Abelmoschus manihot polysaccharide fortifies intestinal mucus barrier to alleviate intestinal inflammation by modulating Akkermansia muciniphila abundance, Acta Pharm Sin B. 14 (2024) 3901-3915. https://doi.org/10.1016/j.apsb.2024.06.002.

[14] P. Giannogonas, A. Apostolou, A. Manousopoulou, et al., Identification of a novel interaction between corticotropin releasing hormone (Crh) and macroautophagy, Sci Rep. 6 (2016) 23342. https://doi.org/10.1038/srep23342.

[15] Y. Bai, Y. Zhou, R. Zhang, et al., Gut microbial fermentation promotes the intestinal anti-inflammatory activity of Chinese yam polysaccharides, Food Chemistry. 402 (2023) 134003. https://doi.org/10.1016/j.foodchem.2022.134003.

[16] I. Prasertsung, K. Aroonraj, K. Kamwilaisak, et al., Production of reducing sugar from cassava starch waste (CSW) using solution plasma process (SPP), Carbohydr Polym. 205 (2019) 472-479. https://doi.org/10.1016/j.carbpol.2018.10.090.

[17] L. Jiang, C. Chi, F. Yuan, et al., Anti-inflammatory effects of anemonin on acute ulcerative colitis via targeted regulation of protein kinase C-theta, Chin Med. 17 (2022) 39. https://doi.org/10.1186/s13020-022-00599-3.

[18] F. Yang, D. Xiao, Y.S. Kim, et al., Synergistic effects of Sargassum horneri polysaccharides and lactic acid bacteria in alleviating DSS-induced colitis and restoring gut homeostasis, Int J Biol Macromol. 321 (2025) 146492. https://doi.org/10.1016/j.ijbiomac.2025.146492.

[19] Q. Qu, Y. Ma, X. Gao, et al., Licorice Total Flavonoids and Its Gut-Enriched Lactobacillus plantarum Synergistically Activate the Nrf2 Pathway to Alleviate Liver Injury, J Agric Food Chem. 73 (2025) 19714-19727. https://doi.org/10.1021/acs.jafc.5c05382.

[20] E. Wiercigroch, E. Szafraniec, K. Czamara, et al., Raman and infrared spectroscopy of carbohydrates: A review, Spectrochim Acta A Mol Biomol Spectrosc. 185 (2017) 317-335. https://doi.org/10.1016/j.saa.2017.05.045.

[21] X.J. Li, S.J. Xiao, J. Chen, et al., Inulin-type fructans obtained from Atractylodis Macrocephalae by water/alkali extraction and immunoregulatory evaluation, Int J Biol Macromol. 230 (2023) 123212. https://doi.org/10.1016/j.ijbiomac.2023.123212.

[22] N.A. Mancilla-Margalli, M.G. Lopez, Water-soluble carbohydrates and fructan structure patterns from Agave and Dasylirion species, J Agric Food Chem. 54 (2006) 7832-7839. https://doi.org/10.1021/jf060354v.

[23] J. Zhang, H. Chen, L. Luo, et al., Structures of fructan and galactan from Polygonatum cyrtonema and their utilization by probiotic bacteria, Carbohydr Polym. 267 (2021) 118219. https://doi.org/10.1016/j.carbpol.2021.118219.

[24] S. Cérantola, N. Kervarec, R. Pichon, et al., NMR characterisation of inulin-type fructooligosaccharides as the major water-soluble carbohydrates from Matricaria maritima (L.), Carbohydrate Research. 339 (2004) 2445-2449. https://doi.org/10.1016/j.carres.2004.07.020.

[25] J. Li, T. Wang, Z. Zhu, et al., Structure Features and Anti-Gastric Ulcer Effects of Inulin-Type Fructan CP-A from the Roots of Codonopsis pilosula (Franch.) Nannf, Molecules. 22(12) (2017) 2258. https://doi.org/10.3390/molecules22122258.

[26] M. Matulova, S. Husarova, P. Capek, et al., NMR structural study of fructans produced by Bacillus sp. 3B6, bacterium isolated in cloud water, Carbohydr Res. 346 (2011) 501-507. https://doi.org/10.1016/j.carres.2010.12.012.

[27] Y. Cheng, S. Tian, Y. Chen, et al., Structural characterization and in vitro fermentation properties of polysaccharides from Polygonatum cyrtonema, Int J Biol Macromol. 258 (2024) 128877. https://doi.org/10.1016/j.ijbiomac.2023.128877.

[28] C. Wang, D. Zhang, M. Zhang, et al., Structural characterization of a novel oligosaccharide from Achyranthes bidentata and its anti-osteoporosis activities, Industrial Crops and Products. 108 (2017) 458-469. https://doi.org/10.1016/j.indcrop.2017.07.018.

[29] P. Zhao, H. Zhou, C. Zhao, et al., Purification, characterization and immunomodulatory activity of fructans from Polygonatum odoratum and P. cyrtonema, Carbohydr Polym. 214 (2019) 44-52. https://doi.org/10.1016/j.carbpol.2019.03.014.

[30] H.Y. Ji, J. Yu, J.S. Jiao, et al., Ultrasonic-Assisted Extraction of Codonopsis pilosula Glucofructan: Optimization, Structure, and Immunoregulatory Activity, Nutrients. 14(5) (2022) 927. https://doi.org/10.3390/nu14050927.

[31] X. Gong, Z. Zhang, X. Shi, et al., Structural elucidation and anti-psoriasis activity of a novel polysaccharide from Saussurea Costus, Carbohydr Polym. 333 (2024) 121963. https://doi.org/10.1016/j.carbpol.2024.121963.

[32] Q. Sun, L. Zhu, Y. Li, et al., A novel inulin-type fructan from Asparagus cochinchinensis and its beneficial impact on human intestinal microbiota, Carbohydr Polym. 247 (2020) 116761. https://doi.org/10.1016/j.carbpol.2020.116761.

[33] L. He, B. Yan, C. Yao, et al., Oligosaccharides from Polygonatum Cyrtonema Hua: Structural characterization and treatment of LPS-induced peritonitis in mice, Carbohydr Polym. 255 (2021) 117392. https://doi.org/10.1016/j.carbpol.2020.117392.

[34] C.X. Dong, L.J. Zhang, R. Xu, et al., Structural characterization and immunostimulating activity of a levan-type fructan from Curcuma kwangsiensis, Int J Biol Macromol. 77 (2015) 99-104. https://doi.org/10.1016/j.ijbiomac.2015.03.009.

[35] Y. Liu, Z. Yu, L. Zhu, et al., Orchestration of MUC2 - The key regulatory target of gut barrier and homeostasis: A review, Int J Biol Macromol. 236 (2023) 123862. https://doi.org/10.1016/j.ijbiomac.2023.123862.

[36] Z.-B. Zhang, C.-Y. Yu, H.-Y. Wang, et al., The history, beneficial ingredients, mechanism, processing, and products of Panax ginseng for medicinal and edible value, Food & Medicine Homology. 2(4) (2025) 9420059. https://doi.org/10.26599/fmh.2025.9420059.

[37] G.-Q. Fu, Y.-X. Li, Y. He, et al., Extraction, structure and bioactivity of Tremella Fuciformis polysaccharides: A review, Food & Medicine Homology. 2(4) (2025) 9420038. https://doi.org/10.26599/fmh.2025.9420038.

[38] L.-F. Jia, P. Chen, G.-D. Qu, et al., A comprehensive review of the sedative-hypnotic mechanisms of edible fungi, Food & Medicine Homology. 2(4) (2025) 9420049. https://doi.org/10.26599/fmh.2025.9420049.

[39] Y. Zhang, W. Ji, H. Qin, et al., Astragalus polysaccharides alleviate DSS-induced ulcerative colitis in mice by restoring SCFA production and regulating Th17/Treg cell homeostasis in a microbiota-dependent manner, Carbohydr Polym. 349 (2025) 122829. https://doi.org/10.1016/j.carbpol.2024.122829.

[40] E.-J. Ning, C.-W. Sun, X.-F. Wang, et al., Artemisia argyi polysaccharide alleviates intestinal inflammation and intestinal flora dysbiosis in lipopolysaccharide-treated mice, Food & Medicine Homology. 1(1) (2024) 9420008 https://doi.org/10.26599/fmh.2024.9420008.

[41] M. Shoaib, A. Shehzad, M. Omar, et al., Inulin: Properties, health benefits and food applications, Carbohydr Polym. 147 (2016) 444-454. https://doi.org/10.1016/j.carbpol.2016.04.020.

[42] C.-y. Wang, P. Fan, N.-X. Yang, et al., Addressing the Precision Delivery Challenges of Food-Medicine Homologous Active Polysaccharides (F-MHAPs): A Synergistic Strategy of "Carrier Adaptation-Targeted Modification-Environmental Response", Food & Medicine Homology. 3(3) (2026) 9420132. https://doi.org/10.26599/FMH.2026.9420132.

[43] M.A. Mensink, H.W. Frijlink, K. van der Voort Maarschalk, et al., Inulin, a flexible oligosaccharide. II: Review of its pharmaceutical applications, Carbohydr Polym. 134 (2015) 418-428. https://doi.org/10.1016/j.carbpol.2015.08.022.

[44] L.M. Vogt, D. Meyer, G. Pullens, et al., Toll-like receptor 2 activation by beta2-->1-fructans protects barrier function of T84 human intestinal epithelial cells in a chain length-dependent manner, J Nutr. 144(7) (2014) 1002-1008. https://doi.org/10.3945/jn.114.191643.

[45] S. Li, L. Wu, T. Wang, et al., Structural elucidation of an active pectin against inflammatory bowel disease from the roots of Sanguisorba officinalis and its protection effect, Carbohydrate Polymers. 388 (2026) https://doi.org/10.1016/j.carbpol.2026.125516.

[46] H. Fan, H. Zhao, Y. Zheng, et al., Polygonati kingianum polysaccharide alleviates dextran sulfate sodium-induced colitis by modulating gut microbiota and metabolic homeostasis, Int J Biol Macromol. 316 (2025) 144836. https://doi.org/10.1016/j.ijbiomac.2025.144836.

[47] M. Qiao, T. Xue, Y. Zhu, et al., Polysaccharides from Cistanche deserticola mitigate inflammatory bowel disease via modulating intestinal microbiota and SRC/EGFR/PI3K/AKT signaling pathways, Int J Biol Macromol. 308 (2025) 142452. https://doi.org/10.1016/j.ijbiomac.2025.142452.

[48] J. Ramirez, F. Guarner, L. Bustos Fernandez, et al., Antibiotics as Major Disruptors of Gut Microbiota, Front Cell Infect Microbiol. 10 (2020) 572912. https://doi.org/10.3389/fcimb.2020.572912.

[49] S. Tiwari, S. Begum, F. Moreau, et al., Autophagy is required during high MUC2 mucin biosynthesis in colonic goblet cells to contend metabolic stress, Am J Physiol Gastrointest Liver Physiol. 321 (2021) G489-G499. https://doi.org/10.1152/ajpgi.00221.2021.

[50] T.X. Yu, H.K. Chung, L. Xiao, et al., Long Noncoding RNA H19 Impairs the Intestinal Barrier by Suppressing Autophagy and Lowering Paneth and Goblet Cell Function, Cell Mol Gastroenterol Hepatol. 9(4) (2020) 611-625. https://doi.org/10.1016/j.jcmgh.2019.12.002.

[51] S.Z. Xie, Z.Z. Shang, Q.M. Li, et al., Dendrobium huoshanense polysaccharide regulates intestinal lamina propria immune response by stimulation of intestinal epithelial cells via toll-like receptor 4, Carbohydr Polym. 222 (2019) 115028. https://doi.org/10.1016/j.carbpol.2019.115028.

[52] W. Liao, D. Cao, Y. Wang, et al., 1,3-and 1,4-linked polysaccharides uptake in intestinal cells relies on clathrin/dynamin 1/Rab5-dependent endocytosis, Nat Commun. 17 (2026) 1831. https://doi.org/10.1038/s41467-026-68542-w.